The declining uptake rate of atmospheric CO2 by land and ocean sinks

M. R. Raupach, M. Gloor, J. L. Sarmiento, J. G. Canadell, T. L. Frölicher, T. Gasser, R. A. Houghton, C. Le Quéré, C. M. Trudinger

Biogeosciences, 11, 3453–3475, 2014
www.biogeosciences.net/11/3453/2014/
doi:10.5194/bg-11-3453-2014

Biogeosciences Open Access

The declining uptake rate of atmospheric CO_2 by land and ocean sinks

M. R. Raupach[1,2,3], M. Gloor[4], J. L. Sarmiento[5], J. G. Canadell[1,2], T. L. Frölicher[5,6], T. Gasser[7,8], R. A. Houghton[9], C. Le Quéré[10], and C. M. Trudinger[11]

[1]CSIRO, Centre for Australian Weather and Climate Research, Canberra, ACT 2601, Australia
[2]Global Carbon Project, CSIRO Marine and Atmospheric Research, Canberra, ACT 2601, Australia
[3]Present affiliation: Climate Change Institute, Australian National University, Canberra, ACT 2601, Australia
[4]School of Geography, University of Leeds, Woodhouse Lane LS9 2JT, UK
[5]Program in Atmospheric and Oceanic Sciences, Princeton University, Sayre Hall, Forrestal Campus, Princeton, NJ 08540-6654, USA
[6]Environmental Physics, Institute of Biogeochemistry and Pollutant Dynamics, ETH Zürich, Switzerland
[7]Centre International de Recherche en Environnement et Développement, CNRS-CIRAD-EHESS-AgroParisTech-PontsParisTech, Campus du Jardin Tropical, 94736 Nogent-sur-Marne Cedex, France
[8]Laboratoire des Sciences du Climat et de l'Environnement, CEA-CNRS-UVSQ, CE l'Orme des Merisiers, 91191 Gif-sur-Yvette Cedex, France
[9]Woods Hole Research Center, Falmouth, MA 02540, USA
[10]Tyndall Centre for Climate Change Research, University of East Anglia, Norwich NR4 7TJ, UK
[11]CSIRO, Centre for Australian Weather and Climate Research, Aspendale, VIC 3195, Australia

Correspondence to: M. R. Raupach (michael.raupach@anu.edu.au)

Received: 26 October 2013 – Published in Biogeosciences Discuss.: 27 November 2013
Revised: 18 April 2014 – Accepted: 29 April 2014 – Published: 2 July 2014

Abstract. Through 1959–2012, an airborne fraction (AF) of 0.44 of total anthropogenic CO_2 emissions remained in the atmosphere, with the rest being taken up by land and ocean CO_2 sinks. Understanding of this uptake is critical because it greatly alleviates the emissions reductions required for climate mitigation, and also reduces the risks and damages that adaptation has to embrace. An observable quantity that reflects sink properties more directly than the AF is the CO_2 sink rate (k_S), the combined land–ocean CO_2 sink flux per unit excess atmospheric CO_2 above preindustrial levels. Here we show from observations that k_S declined over 1959–2012 by a factor of about 1/3, implying that CO_2 sinks increased more slowly than excess CO_2. Using a carbon–climate model, we attribute the decline in k_S to four mechanisms: slower-than-exponential CO_2 emissions growth ($\sim 35\,\%$ of the trend), volcanic eruptions ($\sim 25\,\%$), sink responses to climate change ($\sim 20\,\%$), and nonlinear responses to increasing CO_2, mainly oceanic ($\sim 20\,\%$). The first of these mechanisms is associated purely with the trajectory of extrinsic forcing, and the last two with intrinsic, feedback responses of sink processes to changes in climate and atmospheric CO_2. Our results suggest that the effects of these intrinsic, nonlinear responses are already detectable in the global carbon cycle. Although continuing future decreases in k_S will occur under all plausible CO_2 emission scenarios, the rate of decline varies between scenarios in non-intuitive ways because extrinsic and intrinsic mechanisms respond in opposite ways to changes in emissions: extrinsic mechanisms cause k_S to decline more strongly with increasing mitigation, while intrinsic mechanisms cause k_S to decline more strongly under high-emission, low-mitigation scenarios as the carbon–climate system is perturbed further from a near-linear regime.

Published by Copernicus Publications on behalf of the European Geosciences Union.

1 Introduction

The properties of natural land and ocean CO_2 sinks have major implications both for climate mitigation goals and for adaptive responses. The CO_2 airborne fraction (AF, the fraction of total anthropogenic CO_2 emissions from fossil fuels and net land use change that accumulates in the atmosphere) determines the fraction of emissions that contribute to rising atmospheric CO_2 concentrations, with the remainder (the sink fraction, SF $= 1-$AF) being absorbed by land and ocean sinks.

Since the commencement of high-quality atmospheric CO_2 measurements in 1958, the AF has averaged about 0.44 (Canadell et al., 2007; Knorr, 2009; Le Quéré et al., 2009; Tans, 2009; Ballantyne et al., 2012), with significant interannual variability (Keeling and Revelle, 1985). This fact is one of the most important attributes of the contemporary carbon cycle, with major policy implications both for the climate mitigation challenge and also for adaptation to climate change. The natural CO_2 sinks that absorb more than half of all anthropogenically emitted CO_2 represent a massive ecosystem service to humankind (Millennium Ecosystem Assessment, 2005), with implications that are directly quantified by the AF (Raupach et al., 2008). The mean AF and its possible past and future trends are therefore important, for both biophysical and policy reasons.

The basic reason for the approximate past constancy of the AF is well known: a constant or zero-trend AF would be expected under a "LinExp" idealisation of the carbon cycle, in which land and ocean CO_2 sinks increase linearly with excess CO_2 above preindustrial concentrations (assumption "Lin") and total anthropogenic CO_2 emissions increase exponentially ("Exp") (Bacastow and Keeling, 1979; Hofmann et al., 2009; Tans, 2009; Gloor et al., 2010; Raupach, 2013). This idealisation is a reasonable first approximation to the past behaviour of the carbon cycle, where total CO_2 emissions (both annual and cumulative) have increased roughly exponentially for more than a century, and sinks have increased roughly linearly with excess CO_2.

However, the LinExp idealisation – despite its utility in explaining the observed approximate constancy of the AF – is imperfect even for the past, and is likely to become more so in the future. Several analyses (Canadell et al., 2007; Raupach et al., 2008; Le Quéré et al., 2009) have detected a small increasing trend in the AF since 1958 at a mean relative growth rate around 0.2 to 0.3 % year^{-1}, with significance (probability of positive trend) in the range 0.8 to 0.9. Methodological issues have been raised to question this result, concerning trend detection methods (Knorr, 2009), data (Ballantyne et al., 2012; Francey et al., 2010) and uncertainty analyses (Ballantyne et al., 2012). Nevertheless, multiple studies find results for the magnitude and significance of the AF trend that are in approximate agreement when consistent definitions are used (Canadell et al., 2007; Knorr, 2009; Le Quéré et al., 2009; Ballantyne et al., 2012).

Although the AF and its trend are important metrics of the behaviour of the carbon cycle with direct policy implications, they do not provide unambiguous information about the behaviour or "efficiency" of CO_2 sinks. The main reason is that AF mixes information about sinks and anthropogenic emissions, since AF $= 1 -$ sinks/emissions. For example, under the LinExp idealisation, an AF trend appears when emissions increase non-exponentially, even when sinks are linear in excess CO_2 and thus have a constant efficiency (Gloor et al., 2010).

Recognising these issues with the interpretation of the AF, we here provide an attribution of observed CO_2 sink behaviour over the last 50 years by using a novel observable diagnostic, the CO_2 sink rate. This is a more direct measure of sink efficiency than the AF and offers complementary insights into carbon cycle behaviour, although the two quantities are related and are both obtained from the same observations. We compare the observed past behaviours, likely future trajectories and diagnostic properties of the sink rate and the AF.

2 Theory

2.1 CO_2 mass balance and airborne fraction

The atmospheric CO_2 mass balance is

$$\mathrm{d}c_\mathrm{A}/\mathrm{d}t = (f_\mathrm{Foss} + f_\mathrm{LUC}) \; + \; (f_\mathrm{L} + f_\mathrm{M}), \tag{1}$$

or in more compact form

$$c'_A \; = \; f_\mathrm{E} - f_{\downarrow\mathrm{S}}. \tag{2}$$

Here $c_\mathrm{A} = 2.127\left([\mathrm{CO_2}] - [\mathrm{CO_2}]_\mathrm{q}\right)$ is the excess CO_2 in Pg C (where $[CO_2]$ is the CO_2 mixing ratio in ppm, and $[CO_2]_\mathrm{q} = 278$ ppm is $[CO_2]$ at preindustrial equilibrium); a prime denotes differentiation with respect to time (t), so that $c'_\mathrm{A} = \mathrm{d}c_\mathrm{A}/\mathrm{d}t$ is the atmospheric CO_2 accumulation (in Pg C year^{-1}); $f_\mathrm{E} = f_\mathrm{Foss} + f_\mathrm{LUC}$ is the total CO_2 emission flux, the sum of emissions from fossil fuels and other industry (f_Foss) and from net land use change (f_LUC); and $f_{\downarrow\mathrm{S}} = -f_\mathrm{L} - f_\mathrm{M}$ is the total (land plus ocean) CO_2 sink flux, the negative sum of the land–air (f_L) and ocean–air (f_M, marine) exchange fluxes. All fluxes are in units of Pg C year^{-1} and are positive upward (surface to atmosphere), except for $f_{\downarrow\mathrm{S}}$, which is positive downward to denote a CO_2 sink.

The airborne and sink fractions are the dimensionless quantities

$$\mathrm{AF} \; = \; c'_\mathrm{A}/f_\mathrm{E}, \quad \mathrm{SF} \; = \; f_{\downarrow\mathrm{S}}/f_\mathrm{E} = 1 - \mathrm{AF}. \tag{3}$$

The AF is often alternatively defined as an "apparent airborne fraction" $c'_\mathrm{A}/f_\mathrm{Foss}$ (Oeschger et al., 1980); the definition used here allows the anthropogenic contribution to CO_2 growth from net land use change to be distinguished from the terrestrial carbon sink (Raupach et al., 2008; Le Quéré et al., 2009; Gasser and Ciais, 2013).

Analogous to the AF, the land fraction (LF) and ocean fraction (OF) of total CO_2 emissions are defined by

$$\mathrm{LF} = f_\mathrm{L}/f_\mathrm{E}, \quad \mathrm{OF} = f_\mathrm{M}/f_\mathrm{E} \tag{4}$$

such that $\mathrm{AF}+\mathrm{LF}+\mathrm{OF}=1$ from the atmospheric CO_2 mass balance.

2.2 CO_2 sink rate

The CO_2 uptake rate by land and ocean sinks (k_S, henceforth called the CO_2 sink rate) is the combined land–ocean CO_2 sink flux ($f_{\downarrow\mathrm{S}}$) per unit mass of excess atmospheric CO_2 above preindustrial concentrations (c_A). It is defined (Raupach 2013) by

$$k_\mathrm{S} = f_{\downarrow\mathrm{S}}/c_\mathrm{A} \tag{5}$$

and has dimension 1/time. This definition has two simple (and related) physical interpretations: k_S is the sink strength per unit excess CO_2, and equivalently the instantaneous fractional rate of decrease in excess CO_2 caused by sinks alone. Both lead to the interpretation of k_S as a measure of "sink efficiency" (Gloor et al., 2010).

Several important properties follow from the definition of k_S. First, Eqs. (2) and (5) imply that

$$k_\mathrm{S} = \left(f_\mathrm{E} - c'_A\right)/c_\mathrm{A}. \tag{6}$$

Therefore, k_S (like the AF and SF) can be readily observed using basic data on global CO_2 emissions and concentrations. The simple relationship between k_S, the SF and the AF is

$$k_\mathrm{S} = \mathrm{SF}\, f_\mathrm{E}/c_\mathrm{A} = (1-\mathrm{AF})\, f_\mathrm{E}/c_\mathrm{A}. \tag{7}$$

Second, the definition of k_S can also be written as

$$k_\mathrm{S} = (-f_\mathrm{L} - f_\mathrm{M})/c_\mathrm{A} = k_\mathrm{L} + k_\mathrm{M} \tag{8}$$

with $k_\mathrm{L} = -f_\mathrm{L}/c_\mathrm{A}$ and $k_\mathrm{M} = -f_\mathrm{M}/c_\mathrm{A}$. Thus, k_S can be split into additive components k_L and k_M for land and ocean sinks, respectively, as for the LF and OF (Eq. 4). Similar decompositions are possible for the regional sub-components of the land and ocean sinks.

Third, k_S depends directly on the sink flux and only indirectly (and weakly) on emissions trajectories through their effect on excess CO_2. By contrast, the AF is directly affected as much by a change in emissions as a change in sinks (Gloor et al., 2010). Therefore k_S is a more appropriate diagnostic for sink properties than the AF.

Fourth, a trend in k_S indicates a difference in the relative growth rates of sinks and excess CO_2. The relative growth rate (RGR) of a quantity is its absolute growth rate normalised by its mean, with dimension 1/time; thus, the RGR of a time series $X(t)$ is $\mathrm{RGR}(X) = \langle \mathrm{d}(\ln X)/\mathrm{d}t\rangle \approx \langle X\rangle^{-1}\langle \mathrm{d}X/\mathrm{d}t\rangle$, where angle brackets denote expected values. The evaluation and properties of RGRs are summarised in Appendix A; one important property is that the RGR of a product (or quotient) is the sum (or difference) of the RGRs of its factors (Eq. A3). Combining this with Eq. (5), the relative growth rate of k_S can be written as

$$\mathrm{RGR}(k_\mathrm{S}) = \mathrm{RGR}\left(f_{\downarrow\mathrm{S}}\right) - \mathrm{RGR}(c_\mathrm{A}). \tag{9}$$

Thus, k_S increases (has a positive RGR) when the RGR for sinks exceeds that for excess CO_2, and vice versa.

Fifth, k_S constitutes an observable weighted mean of the multiple timescales governing the global carbon cycle, describing their composite effect at any one time on excess atmospheric CO_2. It is well known that there is no single lifetime for atmospheric CO_2, because the carbon cycle includes multiple processes with timescales from days to millennia (Archer et al., 2009). Describing these processes is a fundamental challenge for carbon cycle modelling. A linearised, multi-pool carbon cycle model is equivalent to a pulse response function for atmospheric CO_2 (the airborne fraction after time t of a pulse of CO_2 into the atmosphere) of the form of a sum of exponentials: $G(t) = \sum a_m \exp(-\lambda_m t)$, where the sum is over a set of modes m with turnover rates λ_m and weights a_m (Li et al., 2009; Joos et al., 2013; Raupach, 2013). The modes are a set of independent carbon pools $z_m(t)$, superpositions of physical carbon pools, that sum to the atmospheric excess carbon $c_\mathrm{A}(t)$. It can be shown (see Appendix B, Eq. B8) that

$$k_\mathrm{S} = \sum_m b_m \lambda_m, \tag{10}$$

where b_m is the fraction of c_A in mode m, summing over m to 1. Thus, k_S is a weighted sum of the turnover rates λ_m, where the weights b_m are time-dependent in linearised, pulse-response-function models of the carbon cycle, and the rates λ_m are also time-dependent in nonlinear models. Equation (10) shows how k_S aggregates the effects of multiple processes with different rates to determine the net drawdown rate of atmospheric CO_2 by sinks at any particular time.

Sixth, under the LinExp idealisation defined in Sect. 1, both k_S and the AF are constant in time (Raupach, 2013; also Bacastow and Keeling, 1979, for the AF only). Conversely, neither k_S nor the AF are constant if CO_2 sinks are nonlinear in excess CO_2 (departure from "Lin") or emissions are non-exponential (departure from "Exp").

3 Estimation of trends

Monthly trajectories for AF and k_S from January 1959 to December 2012 (henceforth 1959.0–2013.0) are shown in Fig. 1. These were obtained from collated data (Le Quéré et al., 2013) on CO_2 emissions from fossil fuels (f_Foss) and net land use change (f_LUC), together with global atmospheric CO_2 concentrations; see Appendix C1 for details and references to primary sources.

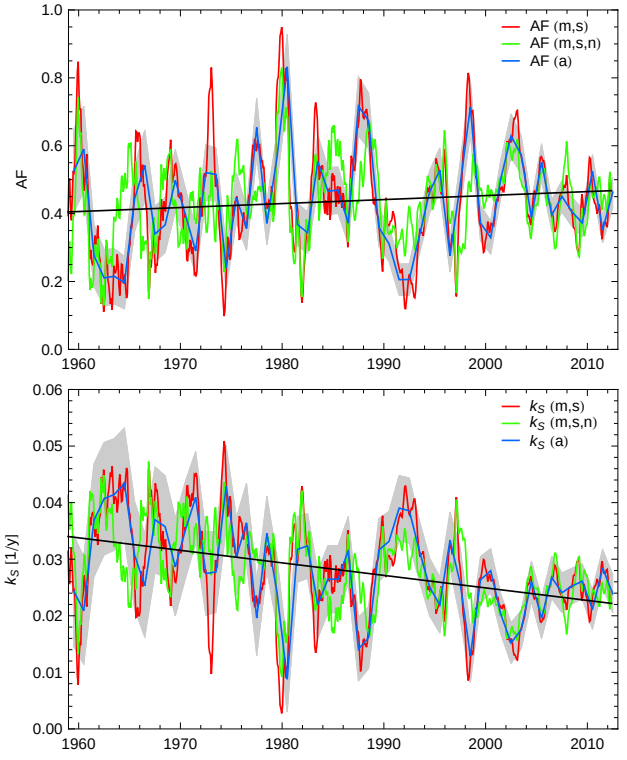

Figure 1. Upper panel: (red) monthly airborne fraction AF(m,s) with 15-month running-mean smoothing, (green) AF(m,s,n) with removal of noise correlated with El Niño–Southern Oscillation (ENSO), (blue) annual AF(a), and (black) best-estimate trend line from AF(m,s,n) with the combined method. Lower panel: (red) monthly CO_2 sink rate $k_S(m,s)$ with 15-month running-mean smoothing, (green) monthly $k_S(m,s,n)$ with ENSO-correlated noise removal, (blue) annual $k_S(a)$, and (black) best-estimate trend line from $k_S(m,s,n)$ with the combined method. Grey bands indicate $\pm1\sigma$ ranges due to observation uncertainties in emissions and CO_2 concentrations, referenced to annual (a) series.

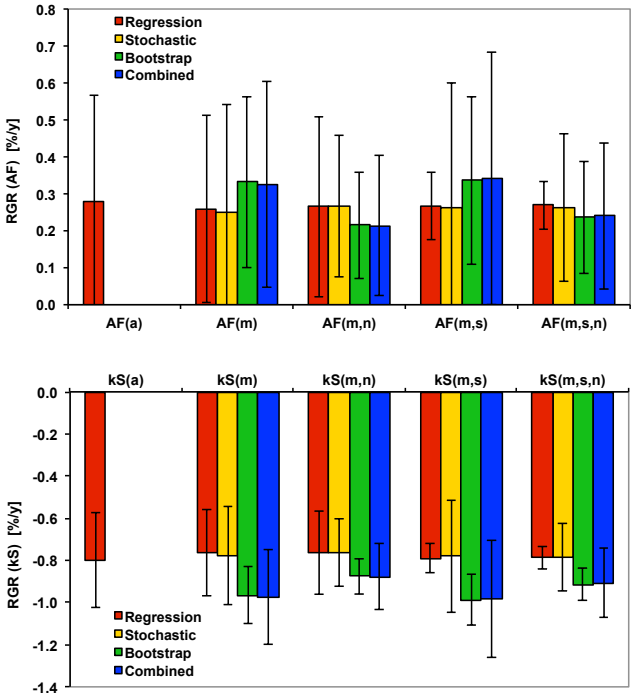

Figure 2. Estimates of RGR(AF) and RGR(k_S) over 1959.0–2013.0, from five data treatments and four trend estimation methods. Error bars show $\pm1\sigma$ confidence intervals. Trends are estimated using Eq. (A2). P values for trend significance are given in Tables 1 and 2. Data treatments are described in detail in Appendix C1, and trend estimation methods in Appendix A. Best trend estimates in the text are from the combined method applied to data treatment (m,s,n), the rightmost blue bar in each panel.

To quantify trends in AF and k_S, we used several different data treatments (Appendix C2) and trend estimation methods (Appendix C3). Our measure of trend is the relative growth rate (Appendix A).

For AF, our best trend estimate (Fig. 2 and Table 1) is RGR(AF) $= 0.24 \pm 0.20\,\%\,\text{year}^{-1}$ ($\pm1\sigma$, $P = 0.89$) about a mean $\langle \text{AF} \rangle$ of 0.44 over 1959.0–2013.0, where $\pm1\sigma$ denotes a 1-standard-deviation confidence interval, and the significance (P) is the probability of positive trend. Both the trend and its significance are comparable with earlier studies cited in the Introduction, when consistent definitions are used; in particular, the statistical significance of the AF trend is found by all studies (including this one) to be less than 95 %, between "likely" and "very likely" in the standard terminology of the Intergovernmental Panel on Climate Change (IPCC, 2007).

For k_S, the best trend estimate (Fig. 2 and Table 2) is RGR(k_S) $= -0.91 \pm 0.17\,\%\,\text{year}^{-1}$ ($\pm1\sigma$, $P > 0.999$ for negative trend), about a mean $\langle k_S \rangle$ of 0.028 $(= 1/36)\,\text{year}^{-1}$. The observed decreasing trend in k_S is statistically robust and "virtually certain" in IPCC terminology, in contrast with the AF trend.

The above uncertainty estimates for trends in AF and k_S reflect variability associated with CO_2 growth rate, but not uncertainties in CO_2 emissions from fossil fuels (f_{Foss}) and net land use change (f_{LUC}). As described in Appendix D, these uncertainties were assessed by repeating the estimation of RGR(AF) and RGR(k_S) with 3 alternative f_{Foss} trajectories (Francey et al., 2010; Gregg et al., 2008; Guan et al., 2012) (Fig. D1) and 11 alternative f_{LUC} trajectories (Le Quéré et al., 2009) (Fig. D3). The resulting trend estimates are statistically indistinguishable from our best estimates.

The RGR of a time series $X(t) > 0$ can be estimated in two ways, as $\text{RGR}(X) = \langle \text{d}(\ln X)/\text{d}t \rangle$ and $\text{RGR}(X) \approx \langle X \rangle^{-1} \langle \text{d}X/\text{d}t \rangle$ (Appendix A, Eqs. A1 and A2, respectively). The former definition is the more fundamental because it precisely preserves identities for RGRs of products and quotients (Eq. A3). However it is not usable in practice if the series $X(t)$ includes any negative values (for which $\ln X$ is undefined), so the latter approximate definition must be

Table 1. Estimates of RGR (AF) over 1959.0–2013.0, using Eq. (A2). Rows distinguish different data treatments, columns distinguish different trend estimation methods. Ranges are $\pm 1\sigma$ confidence intervals; P values in brackets give probability of positive trend. The best estimate (from data treatment AF(m, s, n) with the combined trend estimation method) is shown in bold.

	RGR (AF) (% year^{-1})			
	Regression	Stochastic	Bootstrap	Combined
AF(a)	0.28 ± 0.29 ($P = 0.66$)			
AF(m)	0.26 ± 0.25 ($P = 0.69$)	0.25 ± 0.29 ($P = 0.80$)	0.33[a]	0.33 ± 0.28 ($P = 0.87$)
AF(m, n)	0.26 ± 0.24 ($P = 0.72$)	0.27 ± 0.19 ($P = 0.92$)	0.22[a]	0.21 ± 0.19 ($P = 0.86$)
AF(m, s)	0.27[b]	0.26 ± 0.34 ($P = 0.77$)	0.34[a]	0.35 ± 0.36 ($P = 0.85$)
AF(m, s, n)	0.27[b]	0.26 ± 0.20 ($P = 0.90$)	0.24[a]	**0.24 ± 0.20 ($P = 0.89$)**

[a] The bootstrap trend estimation method does not return confidence intervals or P values.
[b] For data treatments involving smoothing of monthly data, AF(m, s) and AF(m, s, n), regression yields spuriously small confidence intervals (not shown) because of temporal autocorrelation of time series.

Table 2. Estimates of RGR (k_S) over 1959.0–2013.0, using Eq. (A2). Rows distinguish different data treatments, columns distinguish different trend estimation methods. Ranges are $\pm 1\sigma$ confidence intervals. All P values (probability of negative trend) exceed 0.998 and are not shown. The best estimate, with $P > 0.999$, is shown in bold.

	RGR (k_S) (% year^{-1})			
	Regression	Stochastic	Bootstrap	Combined
$k_S(a)$	-0.80 ± 0.23			
$k_S(m)$	-0.77 ± 0.20	-0.78 ± 0.23	-0.96[a]	-0.97 ± 0.23
$k_S(m, n)$	-0.76 ± 0.20	-0.76 ± 0.16	-0.88[a]	-0.88 ± 0.16
$k_S(m, s)$	-0.79[b]	-0.78 ± 0.27	-0.99[a]	-0.98 ± 0.28
$k_S(m, s, n)$	-0.79[b]	-0.79 ± 0.16	-0.91[a]	**-0.91 ± 0.17**

[a, b] See Table 1 caption.

used instead, even though the resulting RGR estimates do not exactly satisfy Eq. (A3). The RGR estimates in Tables 1 and 2 are obtained with Eq. (A2) because the input monthly time series change sign. Later we also use estimates from Eq. (A1), in circumstances where it is important that RGR product and quotient identities be satisfied. In practice the difference between the two RGR estimates is less than the statistical uncertainty in either.

4 Attribution of trends

4.1 Approach and model

We attribute trends in AF and k_S by using a nonlinear carbon–climate model that approximately reproduces observed trends in AF and k_S in its full form. By progressively simplifying the model to eventually reach the LinExp idealisation in which all trends are zero, the contributions of different factors to observed trends can be identified.

In general, it must be noted that attribution of an observed effect from multiple processes to individual process contributions is necessarily a modelling exercise (UNFCCC, 2002), with results that are model-dependent and not directly verifiable by observations unless the system can be manipulated experimentally. However, the present approach of progressively removing processes to reach a known analytic approximation has the advantage that two points in a "process space" are well characterised: the real world (which needs to be approximately reproduced by the model for any attribution exercise to be effective) and the simple analytic idealisation. Our choice of model for this exercise is determined by the requirements that (1) it can approximately reproduce observed trends AF and k_S, and (2) it can be reduced to the LinExp idealisation by formal linearisation.

The model is the Simple Carbon–Climate Model (SCCM), a globally aggregated model of the carbon–climate system (Harman et al., 2011; Raupach, 2013; Raupach et al., 2011). Model state variables comprise one atmospheric CO_2 store, two land carbon stores, four perturbation carbon stores in the ocean, the atmospheric concentrations of four major non-CO_2 greenhouse gases (CH_4, N_2O and two representative halocarbons), and three perturbation global temperatures representing heat stores with different turnover rates (Li and Jarvis, 2009). Radiative forcing by aerosols is incorporated via a simple parameterisation based on a proportionality with $f_{\mathrm{Foss}}(t)$, with a time-dependent coefficient. Carbon in the ocean mixed layer is modelled using a pulse response function that emulates the mixing dynamics of

several complex ocean circulation models (Joos et al., 1996). The model ocean–atmosphere CO_2 flux incorporates full, nonlinear ocean carbonate chemistry (Lewis and Wallace, 1998). The model terrestrial biosphere includes a nonlinear dependence of terrestrial net primary production (NPP) on CO_2 concentration to account for CO_2 fertilisation of plant growth, and a nonlinear dependence of heterotrophic respiration on temperature. The effect of volcanic activity on the terrestrial carbon cycle (Jones and Cox, 2001) is included through an enhancement factor for terrestrial NPP that is proportional to a global volcanic aerosol index (Ammann et al., 2003), tested using recent major eruptions.

SCCM does not resolve interannual variability associated with short-term climate fluctuations, regionally specific processes, and climate effects on the carbon cycle beyond those captured by a response to global temperature. In exchange for these simplifications, an important benefit for this work is that SCCM can be linearised analytically (Raupach, 2013), allowing linearisation to be included explicitly as a simplifying step.

4.2 Model–data comparisons

SCCM satisfactorily reproduces observed trends in AF and k_S over 1959.0–2013.0, as shown in Fig. 3 with a comparison between model predictions (red bars) and RGR estimates using Eqs. (A1) and (A2) (black and grey bars, respectively). Of these, the like-with-like comparison is between red and black bars, for which RGRs are calculated for both the model and observations (respectively) using annual data with Eq. (A1). The grey bars show the best RGR estimates (with uncertainties) from Tables 1 and 2, calculated with Eq. (A2); the difference between black and grey bars does not exceed $\pm 1\sigma$ confidence intervals.

Comparisons of model predictions against observed time series of CO_2, temperature, AF and k_S over the period of high-quality CO_2 observations from 1959 onward indicate satisfactory performance for the purpose of attributing trends over this period (Figs. 4 and 5, right panels). In particular, the model reproduces the observed perturbations in AF and k_S due to major volcanic eruptions (indicated by dots in Fig. 5). However, the model does not reproduce interannual climate variability related to El Niño–Southern Oscillation (ENSO) and other interannual climate modes. Also, model performance against data prior to 1959 is weaker than after 1959, for reasons including data quality, lack of account for interdecadal variability in air–ocean CO_2 and heat exchanges, and lack of incorporation of the full range of forcing factors into the model.

4.3 Process attributions

Figure 3 shows the effects on the modelled trends in AF and k_S of successive simplification by removing processes from the model, while leaving all model parameters unchanged.

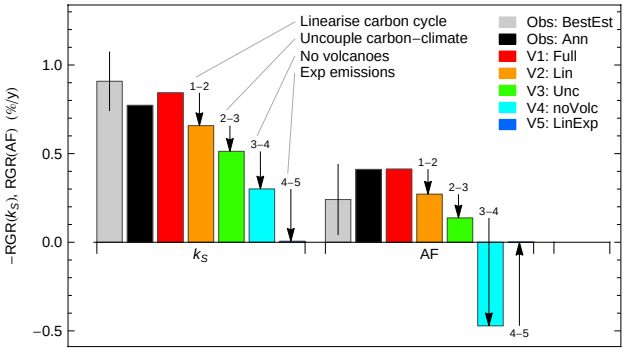

Figure 3. Relative growth rates of k_S and AF over 1959.0–2013.0, at five accumulating levels of model simplification: (V1, red) full model, (V2, orange) linearised, (V3, green) uncoupled, (V4, light blue) no volcanoes, and (V5, dark blue) LinExp idealisation. The labelled vertical arrows indicate the model simplification occurring at each step (e.g. linearisation of the carbon cycle in the step from V1 to V2). Corresponding trajectories of CO_2 and temperature are shown in Fig. 6, and trajectories of k_S and AF in Fig. 7. Note that RGR(k_S) is negative and is plotted with reversed sign. Black bars show observed trends estimated from annual data using Eq. (A1) in Appendix A; these observed trend estimates are directly comparable with model estimates, which were obtained in the same way. Grey bars with $\pm 1\sigma$ confidence intervals are the best trend estimates from Tables 1 and 2, obtained with Eq. (A2). There are small differences between the estimates (within $\pm 1\sigma$ confidence intervals). Reasons for the use of these two different estimation methods are given in the text and in Appendix A.

The first simplification (V1 to V2, where V1 is the full model) is linearisation of the model carbon cycle, using the tangent-linear form of SCCM. This removes all nonlinear dependences of CO_2 fluxes and radiative forcing on carbon stores and temperatures, but retains linearised interactions among these quantities. The result is a reduction in the magnitude of the k_S trend by $\sim 20\,\%$ (noting that RGR(k_S) is negative), most of the reduction being due to removal of nonlinearities associated with the dependence of ocean–air CO_2 exchange on atmospheric CO_2.

The next simplification (V2 to V3) is carbon–climate decoupling, performed by removing all dependences of CO_2 fluxes on temperature through terrestrial NPP, heterotrophic respiration and ocean chemistry (recalling that linearised versions of these interactions were retained in the step from V1 to V2). This simplification also removes all effects of non-CO_2 gases on the carbon cycle, since these are mediated entirely by temperature in this model. This step reduces the magnitude of RGR(k_S) by another $\sim 20\,\%$ of its full-model value.

The third simplification (V3 to V4) is removal of the effects of volcanism on terrestrial NPP. This causes another $\sim 25\,\%$ reduction in the magnitude of RGR(k_S).

The last simplification (V4 to V5) is replacement of real total CO_2 emissions ($f_{Foss} + f_{LUC}$), which depart from

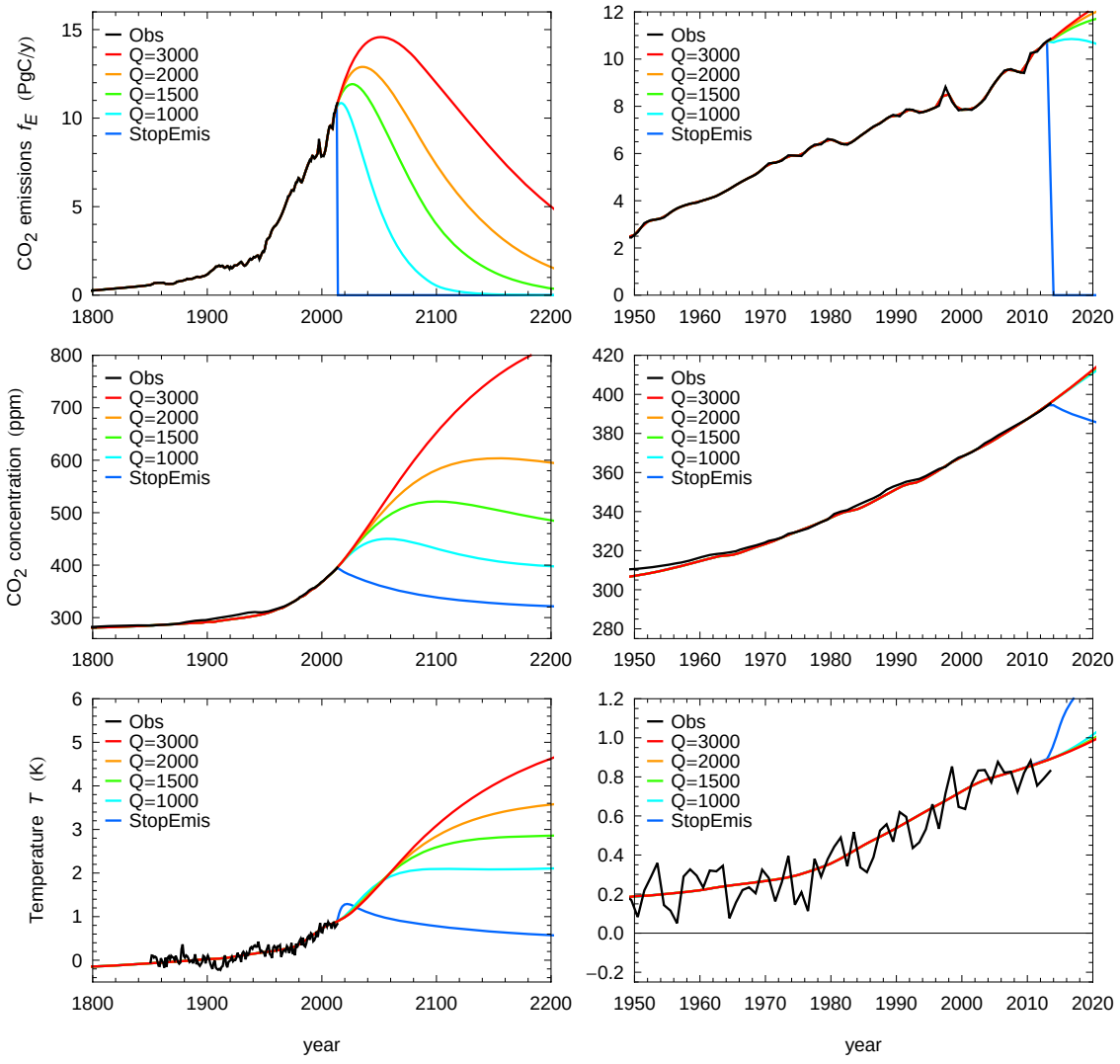

Figure 4. Total CO_2 emissions (f_E, top row) and SCCM predictions for CO_2 concentration (middle row) and temperature (bottom row), with analytic scenarios for future emissions of CO_2 and non-CO_2 gases (CH_4, N_2O, CFCs) such that the all-time cumulative total CO_2 emission Q takes values from 1000 to 3000 Pg C. Scenarios and model details (including treatment of aerosols) are given in Raupach (2013). Left panels show plots against time from 1800 to 2200; right panels zoom in to the period 1950–2020 to compare model with data. This figure is a variation with added detail of Fig. 6 in Raupach (2013).

exponential growth (Gloor et al., 2010; Raupach, 2013), by an exponential trajectory with the same mean growth rate over 1850–2011. This removes the remaining $\sim 35\,\%$ of the magnitude of RGR (k_S). After all four simplification steps, the k_S trend is reduced to zero in the model, consistent with the theoretical requirement of the LinExp idealisation.

We have repeated this progressive model simplification experiment with different orderings for process removal, finding that the above result is independent of ordering to a very good approximation. Not surprisingly, model simplification causes the agreement between model and observations to weaken progressively as processes are removed (Figs. 6 and 7).

The sequence of effects of progressive model simplification is not as simple for the AF trend as for k_S (Fig. 3). For RGR (AF), the largest single change is brought about by removal of volcanic effects: this step alone eliminates the observed positive trend in AF, in accord with other recent findings (Frölicher et al., 2013). In Sect. 5.3 we investigate the reasons for the different responses of RGR (k_S) and RGR (AF) to progressive model simplification, and therefore the different attributions of the observed trends to processes.

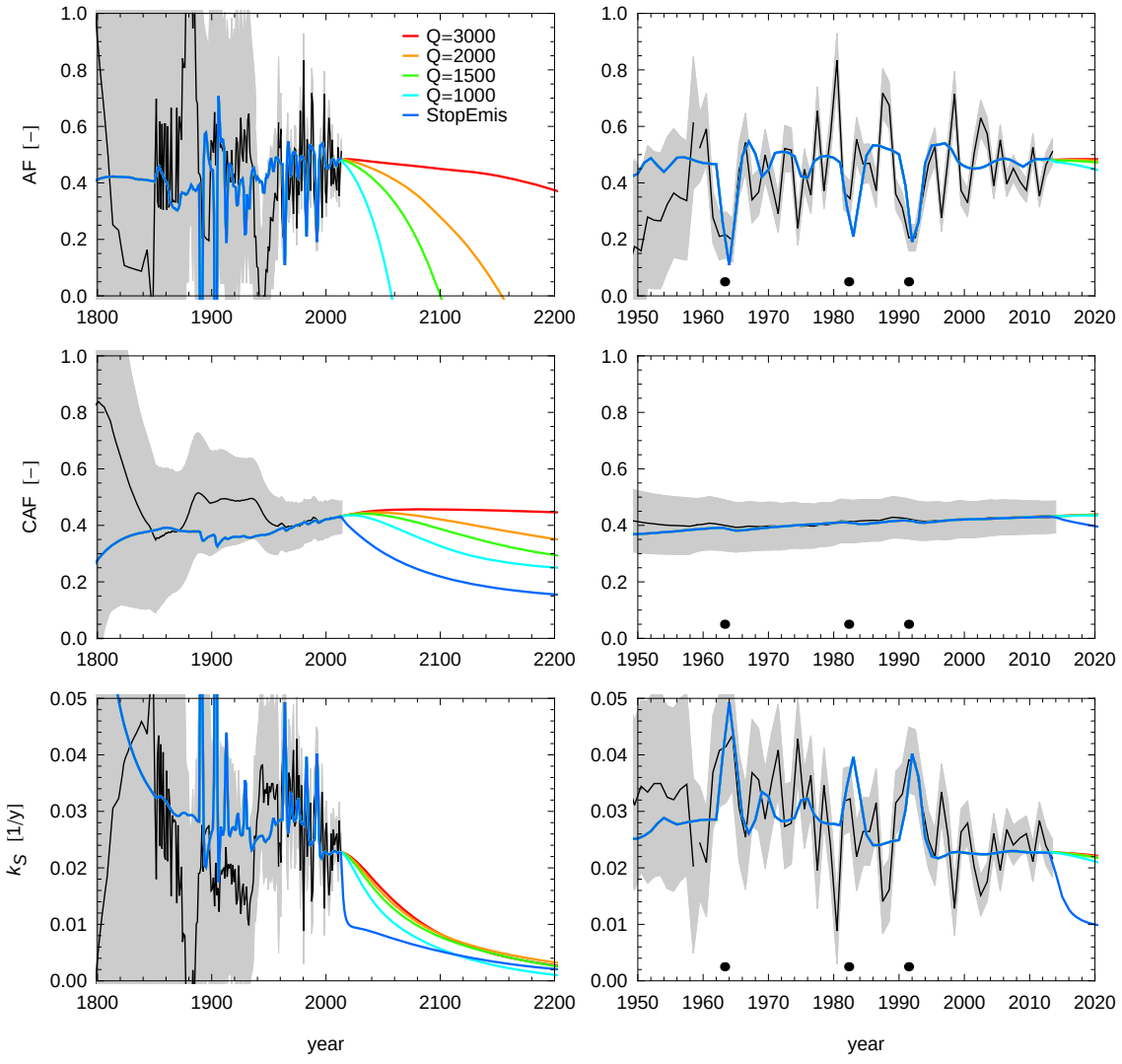

Figure 5. Trajectories of AF and k_S (upper and lower rows) for the analytic scenarios shown in Fig. 4. Dots in right (zoom) panels indicate times of major volcanic eruptions since 1959 (Agung, El Chichon, Pinatubo). Black lines are observations; grey bands indicate $\pm 1\sigma$ ranges due to observation uncertainties in emissions and CO_2 concentrations. Historical SCCM results (prior to 2013.0) appear as blue in all panels. Other details follow Fig. 4. This figure is a variation with added detail of Fig. 7 in Raupach (2013).

5 Discussion

5.1 Extrinsic and intrinsic mechanisms

We have attributed the decline in k_S to four mechanisms. One of these – departure of emissions from exponential growth – is "extrinsic", arising from the trajectory of external anthropogenic forcing of the carbon–climate system. Two others – nonlinear carbon cycle responses to CO_2 and carbon–climate coupling – are "intrinsic", arising from process feedbacks in the system. Volcanic effects are both extrinsic and intrinsic, involving feedbacks triggered by non-anthropogenic forcing from volcanic aerosols.

The primary extrinsic mechanism operates thus: when CO_2 emissions increase more slowly than exponentially, the fast-response, low-capacity modes of the carbon cycle saturate more rapidly than slow modes, so the weights b_m in Eq. (10) decrease with time for faster modes and reciprocally increase for slower modes, causing k_S to decrease. This mechanism is associated with sink capacities through the effect of CO_2 emissions trajectory on the distribution of carbon among the ocean, land and atmospheric stores. It can be described purely by linear theory (Raupach, 2013).

In contrast, the primary intrinsic mechanisms arise from internal feedbacks. Many (though not all) of these are fundamentally nonlinear: prime examples are the dependences of ocean–atmosphere CO_2 fluxes and terrestrial NPP on CO_2,

Table 3. Relative growth rates RGR(AF) and RGR(k_S) over 1959.0–2013.0, with the contributions from the terms in Eqs. (11) and (12), respectively. All growth rates are evaluated with Eq. (A1) and annual data to ensure that the product and quotient rules in Eq. (A3) are satisfied exactly.

Sign	Term	RGR
Total =	RGR(AF)	0.39
(+)	RGR(dc_A/dt)	2.03
(−)	RGR(f_E)	1.64
Total =	RGR(k_S)	−0.77
(+)	RGR(SF)	−0.18
(+)	RGR(f_E)	1.64
(−)	RGR(c_A)	2.23

and the dependence of heterotrophic respiration on temperature. These feedbacks have the net effect of decreasing the turnover rates λ_m in Eq. (10) with increasing CO_2 and temperature, hence decreasing k_S.

5.2 Future behaviours of AF and k_S

Figure 4 (left panels) shows the trajectories of total CO_2 emissions, excess CO_2 and temperature under a set of analytically specified future emission scenarios for all modelled forcing agents; see Appendix B of Raupach (2013) for details. The scenarios are characterised by the parameter Q, the cumulative total CO_2 emission ($f_E = f_{Foss} + f_{LUC}$) integrated from preindustrial times to the far future when emissions decline to zero. This ranges from high emissions (Q = 3000 Pg C) to strong mitigation (Q = 1000 Pg C).

Also shown in Fig. 4 is a "StopEmission" projection for the case where all anthropogenic emissions of CO_2 and other forcing agents are stopped instantly at the present time, taken as 2013.0 for these calculations (Friedlingstein et al., 2011). The temperature projection for this scenario shows a rapid rise in temperature of about 0.5 K as the net cooling radiative forcing from aerosols is switched off suddenly, followed by a slow decline.

The corresponding future behaviour of AF and k_S is shown in Fig. 5 (left panels). Under a high-emissions scenario the AF remains close to its present value for a century or more into the future, while under a strong-mitigation scenario the AF declines fairly rapidly, becoming negative after the time of peak CO_2. For the StopEmission scenario the AF is undefined from the present time onward.

There is continuing decline in k_S under all scenarios. For the StopEmission scenario this decline is initially very rapid, with k_S decreasing to less than half of its present value over a few years as fast modes saturate. Among the scenarios with Q ranging from 1000 to 3000 Pg C, the future rate of decline in k_S varies surprisingly little. This occurs because extrinsic and intrinsic mechanisms respond in opposite ways to changes in emissions: extrinsic mechanisms cause k_S to decline more strongly with increasing mitigation, as emissions trajectories fall progressively further below exponential growth. In contrast, intrinsic mechanisms cause k_S to decline more strongly under high-emission, low-mitigation scenarios as the carbon–climate system is perturbed further from a near-linear regime and rates for individual sink processes decrease. The net result of these opposing influences is that our projected future values (in 2100) of the composite drawdown timescale $1/k_S$ range from ~ 120 to ~ 180 year, for scenarios from emissions-intensive to strong-mitigation (Fig. 5).

5.3 Implications of differing trends in AF and k_S

The proportional effects of the four process-removal steps (Fig. 3, Sect. 4.3) are not the same for RGR(AF) as for RGR(k_S), because these two growth rates depend in different ways upon changes in carbon-cycle fluxes and stores. From Eq. (7), RGR(k_S) can be written as

$$\begin{aligned} \mathrm{RGR}(k_S) &= \mathrm{RGR}(\mathrm{SF}) + \mathrm{RGR}(f_E) - \mathrm{RGR}(c_A) \\ &= \mathrm{RGR}(1-\mathrm{AF}) + \mathrm{RGR}(f_E) - \mathrm{RGR}(c_A)\,, \end{aligned} \tag{11}$$

showing that the growth rate of k_S is a linear combination of the growth rates for SF ($= 1 - \mathrm{AF}$), total emissions (f_E) and excess CO_2 (c_A). The equivalent expression for RGR(AF) is

$$\mathrm{RGR}(\mathrm{AF}) \;=\; \mathrm{RGR}\left(c'_A\right) \;-\; \mathrm{RGR}(f_E)\,. \tag{12}$$

Thus, the growth rate of the AF is a linear combination of the growth rates of atmospheric CO_2 accumulation (c'_A, the time derivative of the excess CO_2) and emissions. The AF increases when CO_2 accumulation grows faster than emissions, and vice versa.

Table 3 shows the contributions to RGR(k_S) and RGR(AF) of the terms in Eqs. (11) and (12), respectively. All growth rates are evaluated using Eq. (A1) to ensure that the product and quotient rules in Eq. (A3) are satisfied exactly. Over 1959.0–2013.0, RGR(k_S) was negative mainly because the growth rate of excess CO_2 $\left(c'_A/c_A\right)$ was significantly larger than the growth rate of total emissions, with a smaller contribution from the growth rate of SF. A positive growth in AF occurred because the growth rate of the CO_2 accumulation $\left(c''_A/c'_A\right)$ exceeded the growth rate of emissions. These different dependencies indicate that there is no direct relationship between the growth rates of AF and k_S, so it is not surprising that the process contributions to the two growth rates are very different (Table 3).

This discussion highlights the different insights obtained from absolute and relative growth rates. CO_2 sinks have unquestionably increased in absolute magnitude since 1959 (Ballantyne et al., 2012); recent work (Sitch et al., 2013) has focussed on quantifying this absolute trend in units of Pg C year^{-2}. However, the increase in sinks ($f_{\downarrow S}$) has been

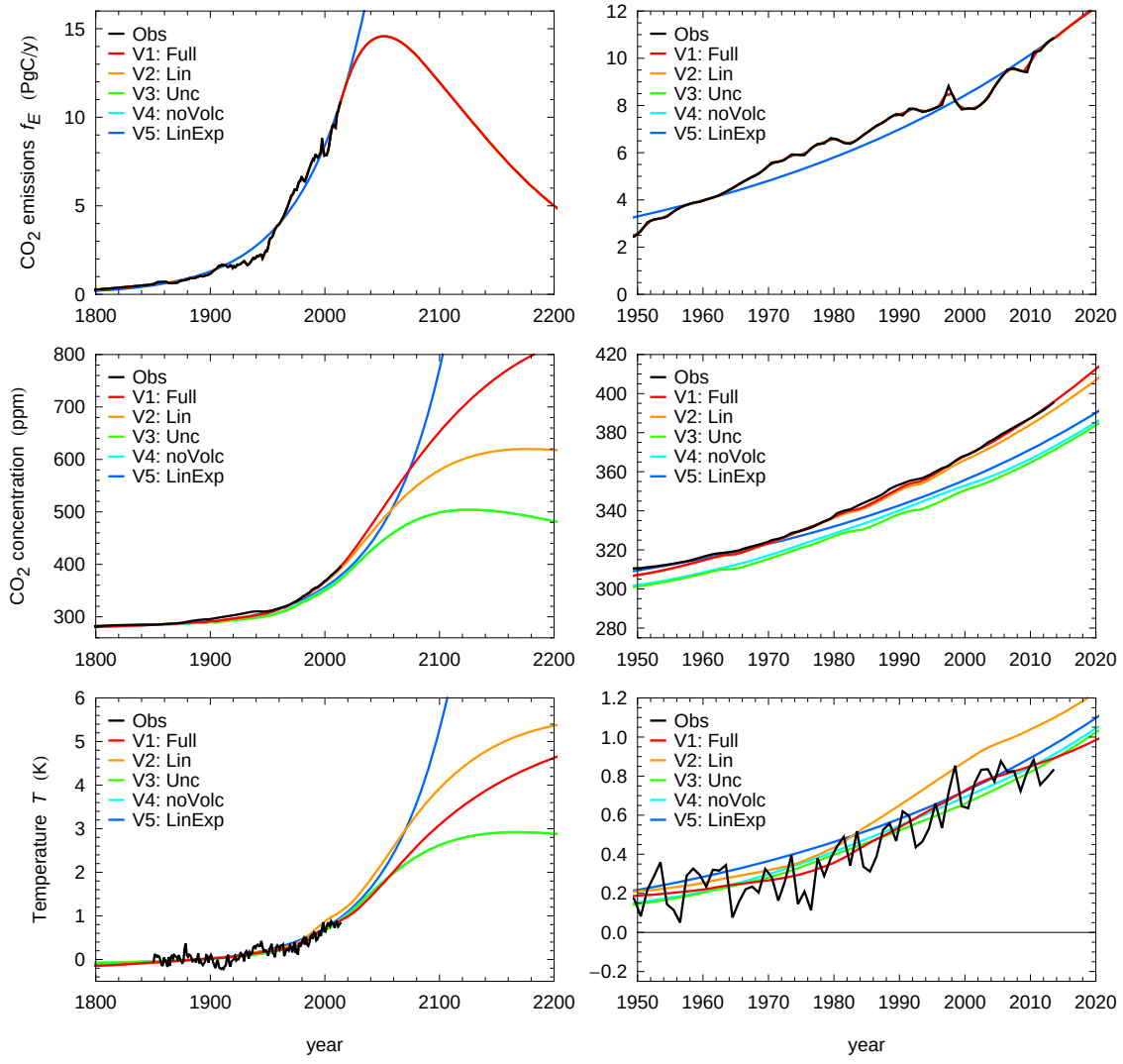

Figure 6. Total CO_2 emissions (f_E, top row) and SCCM predictions for CO_2 concentration (middle row) and temperature (bottom row), at five accumulating levels of model simplification, as in Fig. 3: (1) full model, (2) linearised, (3) uncoupled, (4) no volcanoes, and (5) LinExp idealisation. The emissions scenario is the case $Q = 3000$ Pg C in Fig. 4. Other details follow Fig. 4. This figure is a variation with added detail of Fig. 8 in Raupach (2013), using orderings for model simplification steps consistent with this paper.

accompanied by increases in total emissions (f_E) and atmospheric accumulation (c'_A) (the other terms in the atmospheric CO_2 mass balance, Eq. 2), and also by continuing growth in the excess CO_2 concentration itself (c_A) (Le Quéré et al., 2009, 2013; Fig. C1). Therefore, it is important to investigate not only the absolute growth rate in sinks but also the growth rates of these quantities relative to each other, or which quantities are "winning the race".

Trends in AF, SF and k_S answer this question, with the help of Eqs. (9), (11) and (12). Over 1959.0–2013.0, the positive sign of RGR(AF) indicates that c'_A grew faster than f_E, the negative sign of RGR(SF) indicates that $f_{\downarrow S}$ grew slightly slower than f_E, and the negative sign of RGR(k_S) indicates that $f_{\downarrow S}$ grew slower than excess CO_2 (c_A). This provides a simple rationale for the significance of the relative growth rates.

5.4 Model-independent and model-dependent findings

Many of the findings of this work are wholly or nearly independent of the particular simple model used here (SCCM); rather, they are based on observations or simple analytic inferences. The past decline in k_S follows from observations of CO_2 emissions and accumulation. Attribution of a significant fraction of this decline to extrinsic mechanisms (associated with the effect of emissions trajectory on the distribution of carbon among stores, and thence on sink capacities) is based on robust linear theory, effectively a pulse-response-function

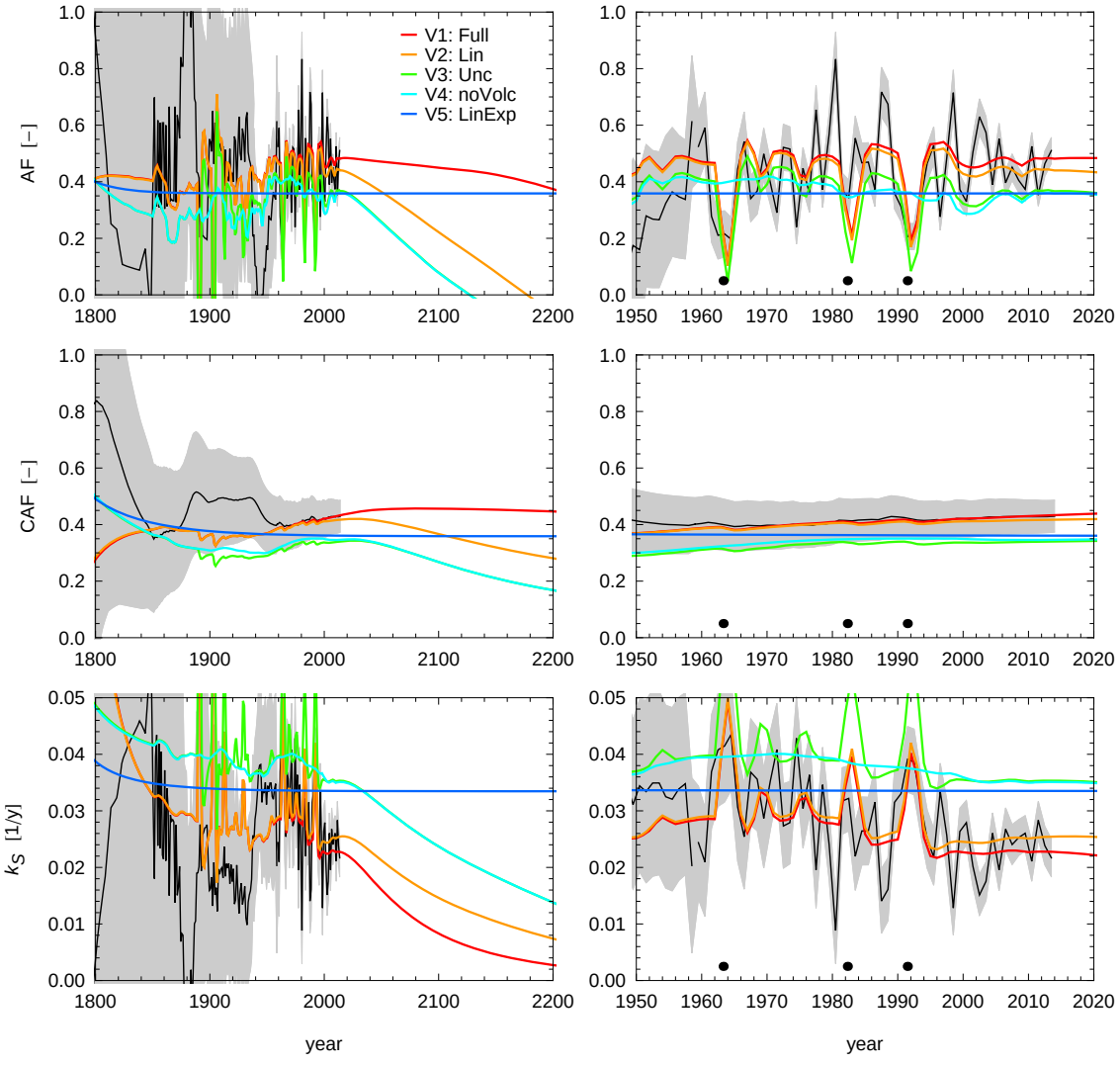

Figure 7. Trajectories of AF and k_S (upper and lower rows) for the model simplification cases shown in Figs. 3 and 6. Dots in right (zoom) panels indicate times of major volcanic eruptions since 1959 (Agung, El Chichon, Pinatubo). Other details as in Figs. 4 and 5. This figure is a variation with added detail of Fig. 9 in Raupach (2013), using orderings for model simplification steps consistent with this paper.

description of the global carbon cycle (Joos et al., 2013; Raupach, 2013). A continued future decline in k_S from extrinsic mechanisms alone is expected from the same linear theory.

Other aspects of our findings are model-dependent, including the precise fractional attributions of the decline in k_S among mechanisms (Fig. 3), which may change as more sophisticated carbon-cycle models are brought to bear on the attribution problem. However, it is important to recognise that any model used in this way, whether simple or complex, must first pass two basic tests: that it includes the processes to be attributed, and that it can reproduce observations well enough for attribution to be possible. These tests are more fundamental than the level of complexity of the model.

As an illustration of the challenge, Figs. 8 and 9 (respectively for AF and k_S) compare the mean and relative growth rate over 1959.0–2013.0 between data, SCCM and the 11 models in the C4MIP intercomparison (Friedlingstein et al., 2006), in both uncoupled and coupled modes. For the growth rate of AF, 7 out of 11 C4MIP models in coupled mode predict the wrong sign (negative rather than positive as observed), and for k_S, the negative growth rate is underestimated by all C4MIP models in coupled mode. For the AF, a similar comparison has been presented previously (Le Quéré et al., 2009); the comparison for k_S is presented here for the first time. The reasons for these discrepancies may partly lie with the fact that the C4MIP protocol did not incorporate volcanism, which has only recently been found to have a large influence on carbon-cycle trends over decades (Frölicher et al., 2013).

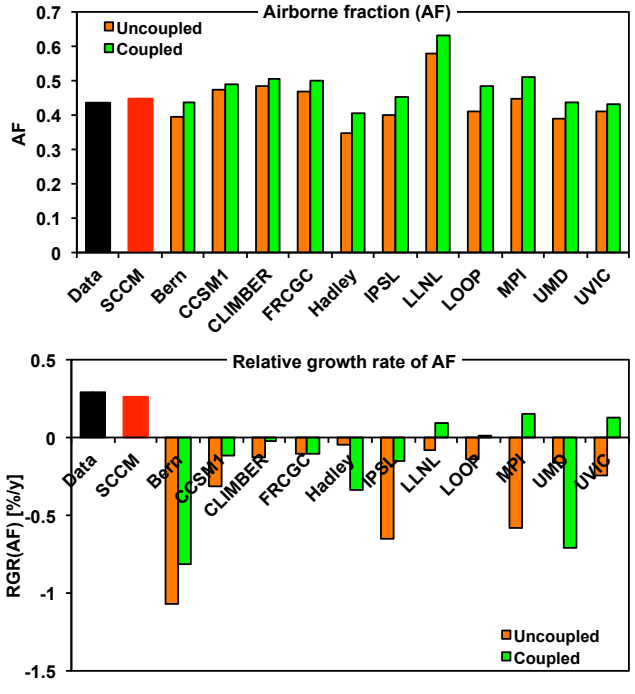

Figure 8. Upper panel: mean AF over 1959.0–2013.0 from data (black bars), SCCM (red bars) and 11 C4MIP models (Friedlingstein et al., 2006) in both uncoupled and coupled modes (orange and green bars, respectively). Lower panel: relative growth rate RGR(AF). For consistency of comparison, all trends are estimated using Eq. (A2) with annual data (the use of Eq. (A2) is necessary because many of the series change sign). This leads to small differences between SCCM trend estimates in Figs. 8 and 3.

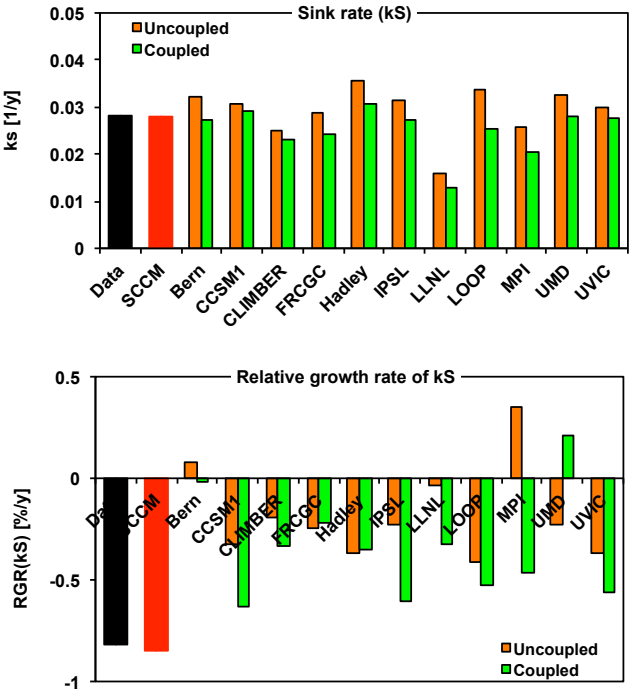

Figure 9. Upper panel: mean sink rate k_S over 1959.0–2013.0 from data (black bars), SCCM (red bars) and 11 C4MIP models (Friedlingstein et al., 2006) in both uncoupled and coupled modes (orange and green bars, respectively). Lower panel: relative growth rate RGR(k_S), estimated using Eq. (A2). See Fig. 8 caption for note on consistency of SCCM trend estimates between Figs. 9 and 3.

6 Conclusions

The implications of this work can be summarised as follows. First, the trajectories of AF and k_S provide different insights into the behaviour of the carbon cycle: trends in the AF indicate differences in the relative growth rates of excess CO_2 accumulation and anthropogenic CO_2 emissions (Eq. 12), while trends in k_S indicate differences in the relative growth rates of sinks and excess CO_2 concentration (Eq. 9). Immediate implications of the observed decline in k_S over 1959.0–2013.0 are that CO_2 sinks increased more slowly than excess CO_2, and that the sink efficiency (the sink strength per unit excess CO_2) decreased.

Second, k_S constitutes an observable weighted mean of the multiple rates λ_m of processes controlling the global carbon cycle, describing their combined effect on excess atmospheric CO_2 through land and ocean sinks (Eq. 10). Over 1959.0–2013.0, the composite drawdown timescale $1/k_S$ increased from ~ 30 to ~ 45 years, and is projected to increase further in future. Therefore the mix of carbon-cycle timescales contributing to drawdown of CO_2 by sinks has shifted observably towards longer scales.

Third, we attribute the observed decline in k_S to four mechanisms: slower-than-exponential CO_2 emissions growth ($\sim 35\,\%$ of the trend); volcanic eruptions ($\sim 25\,\%$); responses of CO_2 sinks to climate change ($\sim 20\,\%$); and nonlinear responses to increasing CO_2, mainly associated with ocean CO_2 sinks ($\sim 20\,\%$). The first of these mechanisms is "extrinsic" (associated with the trajectory of external forcing of the carbon–climate system and its effect on sinks through the distribution of carbon among ocean, land and atmospheric stores). The last two are "intrinsic" (associated with feedback responses of sink processes to changes in climate and atmospheric CO_2). Volcanic effects include both non-anthropogenic extrinsic forcing and intrinsic feedback responses.

Fourth, the observed decline in k_S is projected to continue under all realistic emissions scenarios (Fig. 5). This implies that the shift of the mix of carbon cycle timescales towards longer scales, already evident in past observations, is projected to continue in future. By contrast, future trends in AF are much more strongly dependent on emissions scenarios, with the AF becoming negative under strong-mitigation scenarios.

Fifth, our model-based attribution suggests that the effects of intrinsic mechanisms (carbon-cycle responses to CO_2 and carbon–climate coupling) are already evident in the carbon cycle, together accounting for $\sim 40\,\%$ of the observed decline in k_S over 1959.0–2013.0. These intrinsic mechanisms encapsulate the vulnerability of the carbon cycle to reinforcing system feedbacks. By comparison, the extrinsic, sink-capacity mechanisms are much easier to describe and are captured by pulse-response-function models of the global carbon cycle. An important open question is how rapidly the intrinsic mechanisms and associated feedbacks will contribute to further decline in k_S under various emission scenarios.

Finally, the approach of progressive model simplification used here can be applied to attribute trends in k_S with other suitable models. While our attribution is necessarily restricted to processes resolved in the simple model used here, a more complex model could attribute trends to more finely resolved processes such as regional contributions to land and ocean sinks (Ciais et al., 2013; Sitch et al., 2013). The approach ensures that all contributions sum to the full model trend in k_S. Such an attribution would show not only how different regions contribute to the global ecosystem service provided by land and ocean carbon sinks, as quantified by their additive contributions to the global sink flux or global sink rate k_S, but also how these contributions are changing in different ways in response to both extrinsic (forcing) and intrinsic (feedback) influences.

Appendix A: Properties of the relative growth rate

For a process $X(t)$ with all $X(t) > 0$, the relative growth rate is

$$\mathrm{RGR}(X) = \left\langle \frac{\mathrm{d}\ln X(t)}{\mathrm{d}t} \right\rangle, \tag{A1}$$

where angle brackets denote expected values. However, time series for noisy processes $X(t)$ often have values of both signs – for example, monthly time series of AF and k_S. In this case, Eq. (A1) must be approximated as

$$\mathrm{RGR}(X) \approx \frac{1}{\langle X(t)\rangle} \left\langle \frac{\mathrm{d}X(t)}{\mathrm{d}t} \right\rangle. \tag{A2}$$

Equation (A1) is the more fundamental of the two definitions because it has the important property of automatically satisfying the following identities for relative growth rates of products, quotients and powers of any processes $X(t)$ and $Y(t)$:

$$\left.\begin{array}{lcl} \mathrm{RGR}(XY) & = & \mathrm{RGR}(X) + \mathrm{RGR}(Y) \\ \mathrm{RGR}(X/Y) & = & \mathrm{RGR}(X) - \mathrm{RGR}(Y) \\ \mathrm{RGR}(X^a) & = & a\,\mathrm{RGR}(X). \end{array}\right\} \tag{A3}$$

Relative growth rates calculated with Eq. (A2) do not automatically satisfy these identities. However, in practice for the the AF and k_S, the difference between Eqs. (A1) and (A2) is less that the statistical uncertainty in RGR from either method.

Equation (A2) is used with monthly data for the "best-estimate" RGR values in this paper, because most monthly series have values of both signs. For the attribution of contributions to $\mathrm{RGR}(k_S)$ and $\mathrm{RGR}(\mathrm{AF})$ (Fig. 3, Table 3), Eq. (A1) is used with annual data to ensure that the attributed contributions sum to the total trend.

Appendix B: Sink rate k_S as a weighted mean of turnover rates

Here it is shown that the sink rate k_S is a weighted mean of the turnover rates contributing to a pulse response function for atmospheric CO_2, following previous work (Raupach, 2013) with simplified notation.

At a high level of generality, a linearised, multi-pool model of the carbon cycle is

$$\frac{dc_i}{dt} = f_i(t) - \sum_j K_{ij} c_j(t); \quad c_i(0) = 0, \tag{B1}$$

where $c_i(t)$ is the excess carbon (the perturbation above a preindustrial equilibrium state) in pool i, $f_i(t)$ is the anthropogenic carbon input into pool i, and $\mathbf{K} = K_{ij}$ is a square transfer matrix describing inter-pool transfers. This is a coupled dynamical system that can be solved readily by method of normal modes. The approach is to transform the system to a new frame where the state variables $c_i(t)$ become "normal modes" satisfying independent, uncoupled equations. In the new frame, the atmospheric excess carbon pool c_A can be written as a sum of rescaled normal modes $z_m(t)$:

$$c_A(t) = \sum_m z_m(t). \tag{B2}$$

The modes $z_m(t)$ are linear superpositions of the excess carbon pools $c_i(t)$, governed by

$$\frac{dz_m}{dt} = a_m f_E(t) - \lambda_m z_m; \quad z_m(0) = 0, \tag{B3}$$

where λ_m is the turnover rate for mode m, and a_m is a weight (summing over m to 1) specifying the fraction of total emissions to the atmosphere ($f_E = f_{Foss} + f_{LUC}$) entering mode m. The rates λ_m are the eigenvalues of the transfer matrix $\mathbf{K}$. The solution for $c_A(t)$ is then given by

$$c_A(t) = \int_0^t G(t-\tau) f_E(\tau) d\tau, \tag{B4}$$

where

$$G(t) = \sum_m a_m \exp(-\lambda_m t) \tag{B5}$$

is a pulse response function (PRF) for atmospheric CO_2 (the fraction of an instantaneous pulse of CO_2 into the atmosphere that remains airborne after time t) taking the form of a sum of decaying exponential terms with decay rates λ_m. One of the decay rates is often taken as zero, so that $G(t) = a_0 + a_1 \exp(\lambda_1 t) + \ldots$

Summing Eq. (B3) over modes m, the excess atmospheric CO_2 is governed by

$$\frac{dc_A}{dt} = f_E(t) - \sum_m \lambda_m z_m. \tag{B6}$$

From Eq. (2), the atmospheric CO_2 budget (with the total CO_2 sink expressed using the definition of the sink rate k_S, Eq. 5) is

$$\frac{dc_A}{dt} = f_E(t) - k_S c_A. \tag{B7}$$

Equating the last terms in Eqs. (B6) and (B7), it follows that

$$k_S = \sum_m b_m \lambda_m; \quad b_m = z_m / c_A. \tag{B8}$$

Hence k_S is a weighted mean of the turnover rates λ_m for different modes. The weights b_m are the fractions of c_A appearing in the modes m, and from Eq. (B2), these weights sum to 1.

The weights b_m depend on time in general, because the modes z_m grow at different rates λ_m. If emissions $f_E(t)$ were steady, then z_m for faster modes with larger λ_m would saturate to the equilibrium value $f_{E(steady)}/\lambda_m$ more rapidly than z_m for slower modes. This would cause b_m to give progressively higher relative weight to slower modes as time advances, so that k_S would decrease. In the case where emissions increase exponentially, k_S is constant in time, like the AF. An exponentially increasing trajectory $f_E(t)$ is the only case leading to constant k_S and AF (Raupach, 2013).

Appendix C: Data sources and treatments

C1 Primary data sources

Primary data are as for the global CO_2 budget compiled by the Global Carbon Project to 2011 (Le Quéré et al., 2013), with extensions to 2012 based on primary data sources (Fig. C1). Details are as follows:

Atmospheric CO_2 accumulation: this is the rate of increase in atmospheric CO_2, $c'_A = dc_A/dt$ (in Pg C year^{-1}), where $c_A = 2.127([CO_2] - [CO_2]_q)$ (Sect. 2.1). Three time series for monthly $[CO_2]$ were used: in situ $[CO_2]$ at Mauna Loa (MLO, March 1958 onward), flask $[CO_2]$ at the South Pole (SPO, June 1957 onward), and a globally averaged CO_2 series from multiple stations (GLB, January 1980 onward). MLO and SPO data were from the Scripps Institution of Oceanography (Keeling et al., 2005, 2001; Scripps CO_2 Program, 2013); GLB data were from the Earth Systems Research Laboratory of the National Oceanographic and Atmospheric Administration (NOAA-ESRL, 2013). The series used here were gap-filled and deseasonalised by removal of annual cyclic components. Global mean $[CO_2]$ from March 1958 to December 1979 was estimated as (MLO + SPO)/2, and from January 1980 to January 2011 by the GLB value. The monthly CO_2 growth rate (with annual cycle removed) was calculated from each series by a centred first difference.

CO_2 *emissions:* annual global data on CO_2 emissions from fossil fuels and other industrial processes (f_{Foss}) are from the Carbon Dioxide Analysis and Information Center (CDIAC) at the Oak Ridge National Laboratory, USA (Boden et al., 2013). Data on CO_2 emissions from net land use change (f_{LUC}) are based on a bookkeeping method (Houghton, 2010). Cumulative fossil-fuel emissions ($Q_{Foss}(t)$) were estimated by accumulating $f_{Foss}(t)$ from 1751. Cumulative LUC emissions ($Q_{LUC}(t)$) were estimated by accumulating $f_{LUC}(t)$ from 1751, with backward linear extrapolation from the earliest year of data (1851) to zero in 1751.

C2 Data treatments

The five data treatments for time series of AF were as follows.

1. AF(a) is a simple, untreated annual AF time series: $\mathrm{AF}(a) = (\Delta c_A/\Delta t)/(f_{Foss} + f_{LUC})$ with $\Delta t = 1$ year and discretisation to yield year-centred estimates (e.g. 2009.5); Δc_A is the increment in the atmospheric mass of CO_2 at successive year starts (e.g. 2009.0 to 2010.0), and emissions f_{Foss} and f_{LUC} are year-centred (e.g. 2009.5).

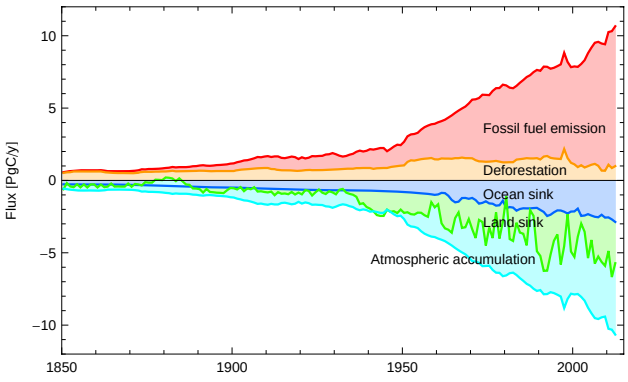

Figure C1. Global atmospheric CO_2 budget for 1959.0–2013.0 (Eq. 1), showing stacked time series of annual f_{Foss}, annual f_{LUC}, annual CO_2 accumulation $c'_A = dc_A/dt$, annual land–air exchange flux f_L, and annual ocean–air exchange flux f_M.

2. AF(m) is a simple, untreated monthly AF time series: $\mathrm{AF}(m) = (\Delta c_A/\Delta t)/(f_{Foss} + f_{LUC})$ with $\Delta t = 1$ month and discretisation to yield 12 month-centred estimates per year (at $2009 + 1/24$, $2009 + 3/24$, …, $2009 + 23/24$). Linear interpolation between annual data points was used to estimate emissions at intervening times, and linear interpolation between monthly data points was used similarly for concentrations.

3. AF(m, s) is a version of the monthly series AF(m) with 15-month running-mean smoothing applied to time series of dc_A/dt before calculation of the AF. This removes most high-frequency (faster than annual) variability (Raupach et al., 2008).

4. AF(m, n) is a monthly AF series without smoothing but with noise reduction by removal of the fluctuating component linearly correlated with El Niño–Southern Oscillation (ENSO) and volcanic aerosol indices. These together account for about half the variance in dc_A/dt from fluctuations shorter than a decade (Raupach et al., 2008). Contributions to the other half of the variance include climate modes other than ENSO, nonlinear effects, and regionally specific effects.

5. AF(m, s, n) is a monthly AF series with both 15-month smoothing as in AF(m, s) and noise reduction as in AF(m, n). Results are insensitive to the order in which smoothing and noise reduction are applied.

For the CO_2 sink rate k_S, similar data treatments were used. This yielded five series: $k_S(a)$, $k_S(m)$, $k_S(m, s)$, $k_S(m, n)$ and $k_S(m, s, n)$.

C3 Trend estimation methods

The four trend estimation methods were as follows.

1. *Linear regression:* simple least-squares linear regression overestimates the confidence in the estimated trend, yielding a spuriously low CI (confidence interval) and spuriously high P value (probability of positive trend) when a series is temporally autocorrelated, as for all our series.

2. *Stochastic method:* this method estimates the confidence interval for the trend with account for the temporal autocorrelation of the time series (Canadell et al., 2007; Le Quéré et al., 2007). For a time series $X(t)$, steps are as follows: (a) the trend X^T is found by conventional least-squares linear regression, yielding a trend line $X^T = x_0 + x_1 t$. (b) The lagged autocorrelation function of the residual $(X - X^T)$ is fitted with an autoregressive (AR) model (Box et al., 1994). To represent the autocorrelation function for monthly data adequately, an AR model of order 20 is used, noting that a good fit to the autocorrelation function is desirable and does not translate into overfitting in the final result because of the stochastic nature of the method. (c) An ensemble of 1000 stochastic realisations of the data is generated with mean trend X^T and residuals correlated as in the AR model. Members of this ensemble have a similar mean trend and autocorrelation function to the original series, but vary stochastically among realisations. (d) The trend for each member of this ensemble is determined by least-squares linear regression, yielding 1000 estimates of the trend (x_1). (e) The probability density function (PDF) of trend estimates x_1 is calculated, yielding trend statistics. The P value is the fraction of the 1000 estimates of x_1 that is greater than 0 for a positive trend, or less than 0 for a negative trend.

3. *Bootstrap method:* both regression and stochastic methods suffer from sensitivity to the choice of start and end times, yielding different results if start or end times are shifted by a few months. The bootstrap method overcomes this problem. An ensemble of time series is constructed by selecting continuous subseries from the original series $X(t)$ with randomised start and end times, subject to the condition that the minimum record length of each ensemble member is at least a fraction f_{Bts} of the complete record. The ensemble is constructed with replacement, so this is a "bootstrap" method. The members of the ensemble are not independent, but represent different possible realisations of the observational constraints determining the length of the series. The choice of f_{Bts} is a compromise between the requirements that (a) ensemble members include most of the original series and (b) the variations in start and end times be enough to randomise their effects. The latter requirement demands that the omitted portions of the record typically encompass several integral timescales for the series $X(t)$. We used $f_{\mathrm{Bts}} = 0.8$. The bootstrap method reduces the influence of the choice of start and end times and therefore yields an improved estimate of mean trend, but provides no estimate of uncertainty information (CI or P value) because the ensemble members are not independent.

4. *Combined method:* here both the stochastic and bootstrap methods are applied together. Steps are as follows: (a) an ensemble of continuous subseries with randomised start and end times is selected as in the bootstrap method. (b) The trend (x_1) for each subseries is determined by linear regression. (c) The lagged autocorrelation function for the entire series is found, as in the stochastic method. (d) Using this autocorrelation function and the trend for each subseries, a stochastic ensemble of series is generated. (e) The trend for each ensemble member is found by linear regression. (f) Statistics of the ensemble of trend estimates are found as in the stochastic method. The combined method provides our best estimates, because it combines the benefits of the bootstrap method for estimation of trend and the stochastic method for confidence interval.

Table D1. Details of AF trend estimates from 11 alternative time series for CO_2 emissions from net land use change, f_{LUC}. Trends are evaluated using Eq. (A2). Data are extrapolated from the last point in each series assuming either "Recent fall" (constant f_{LUC} to 2000 and linear decline from 2000 to 2012 at 0.03 Pg C year^{-1} per year, with the constraint that f_{LUC} not fall below the lesser of the last point and 0.5 Pg C year^{-1}); or "Recent const" (constant f_{LUC} to 2012). Time series are plotted in Fig. D3. The combined trend estimation method is used for all AF trend estimates. Ranges are $\pm 1\sigma$ confidence intervals; P values in brackets give probability of positive trend.

Ident.	No.	Lead author (references in caption)	Carbon cycle model	Land cover data	Last year	RGR (AF) (% year^{-1}) (Recent fall)	RGR (AF) (% year^{-1}) (Recent const)
Hou08	1	Houghton	Houghton	FAO	2008	0.16 ± 0.20 ($P = 0.81$)	0.16 ± 0.20 ($P = 0.81$)
vanMd	2	Van Minnen	IMAGE2	HYDE[a]	2000	0.17 ± 0.20 ($P = 0.82$)	0.15 ± 0.20 ($P = 0.78$)
vanMp	3	Van Minnen	IMAGE2	HYDE[b]	2000	0.20 ± 0.20 ($P = 0.86$)	0.18 ± 0.20 ($P = 0.82$)
IBIS	4	McGuire	IBIS	SAGE	1992	0.23 ± 0.21 ($P = 0.88$)	0.21 ± 0.22 ($P = 0.85$)
HRBM	5	McGuire	HRBM	SAGE	1992	0.26 ± 0.21 ($P = 0.90$)	0.24 ± 0.21 ($P = 0.88$)
LPJ	6	McGuire	LPJ	SAGE	1992	0.41 ± 0.21 ($P = 0.98$)	0.39 ± 0.22 ($P = 0.96$)
TEM	7	McGuire	TEM	SAGE	1992	0.24 ± 0.20 ($P = 0.89$)	0.24 ± 0.20 ($P = 0.89$)
Piao	8	Piao	ORCHIDEE	SAGE	1992	0.22 ± 0.22 ($P = 0.85$)	0.20 ± 0.23 ($P = 0.82$)
ShS1	9	Shevliakova	LM3V	SAGE/HYDE	1990	0.29 ± 0.20 ($P = 0.93$)	0.27 ± 0.21 ($P = 0.91$)
ShH1	10	Shevliakova	LM3V	HYDE	1990	0.20 ± 0.21 ($P = 0.84$)	0.17 ± 0.22 ($P = 0.80$)
Str08	11	Strassmann	BernCC	HYDE	2000	0.25 ± 0.20 ($P = 0.90$)	0.23 ± 0.20 ($P = 0.88$)

[a] Default.
[b] Pasture.
References: Houghton (2010), McGuire et al. (2001), Piao et al. (2009), Shevliakova et al. (2009), Strassmann et al. (2008), Van Minnen et al. (2009).

Appendix D: Implications of uncertainties in emissions

The uncertainty estimates for RGR (AF) and RGR (k_S) in Fig. 2 and Tables 1 and 2 reflect the stochastic variability associated with CO_2 growth rate, but not the uncertainty in data on CO_2 emissions from fossil fuels and other industrial processes (f_{Foss}) and from net land use change (f_{LUC}). These are assessed as follows.

Uncertainty in CO_2 emissions from fossil fuels and other industrial processes (f_{Foss}): the uncertainty in f_{Foss} is estimated as ± 6 % (Andres et al., 2012; Marland, 2008). If this is random, the uncertainty propagated into RGR (AF) and RGR (k_S) is very small. However, some studies have suggested systematic or strongly temporally autocorrelated biases for some countries, notably an underestimate of up to 20 % in the late 1990s to early 2000s for China (Gregg et al., 2008). This would also be consistent with a suggested underestimate of global $f_{Foss} + f_{LUC}$ for this period (Francey et al., 2010). Also, it has been suggested recently that there are significant uncertainties in Chinese emissions, particularly since 2005, from discrepancies between national and summed provincial accounts (Guan et al., 2012).

To assess the consequences of these possible revisions to f_{Foss}, we computed RGR (AF) and RGR (k_S) using three alternative f_{Foss} series (Fig. D1), in which f_{Foss} was increased (1) between 1998 and 2003, (2) between 1993 and 2003, and (3) from 2000 onward using revised Chinese emissions based on provincial rather than national data (Guan et al., 2012). The resulting trends RGR (AF) and RGR (k_S) (Fig. D2), computed using data treatment (m, s, n) and the combined trend detection method, are slightly smaller in magnitude

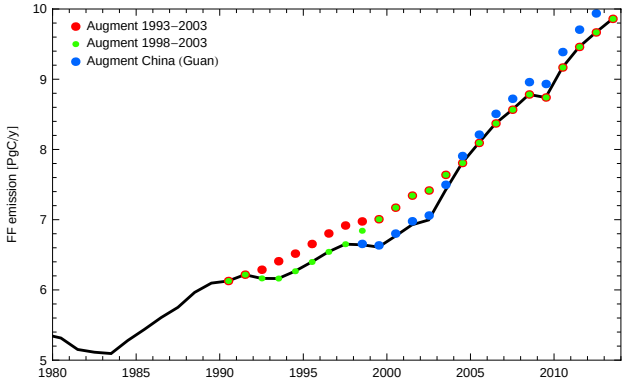

Figure D1. Alternative trajectories for global CO_2 emissions from fossil fuels and other industrial sources (f_{Foss}): (black) primary data, (red dots) f_{Foss} augmented by 3 % from 1993 to 1998 and 6 % between 1999 and 2003 (with tapering), (green dots) f_{Foss} augmented by 6 % between 1998 and 2003 (with tapering), and (blue dots) f_{Foss} if recent Chinese emissions are revised upward to use summed provincial rather than national data (Guan et al., 2012) (their Fig. 2). The trajectories shown by red and green dots follow suggestions of global emissions underestimates in the 1990s to early 2000s (Francey et al., 2010).

than the best estimates with primary f_{Foss} data, but the differences are not statistically significant. Therefore, our conclusions are unaffected by any of the three possible revisions to f_{Foss} (all of which are still speculative).

Uncertainty in CO_2 emissions from net land use change (f_{LUC}): it is well known that uncertainty in f_{LUC} is significant (Houghton, 2010, 2003) and propagates into the largest

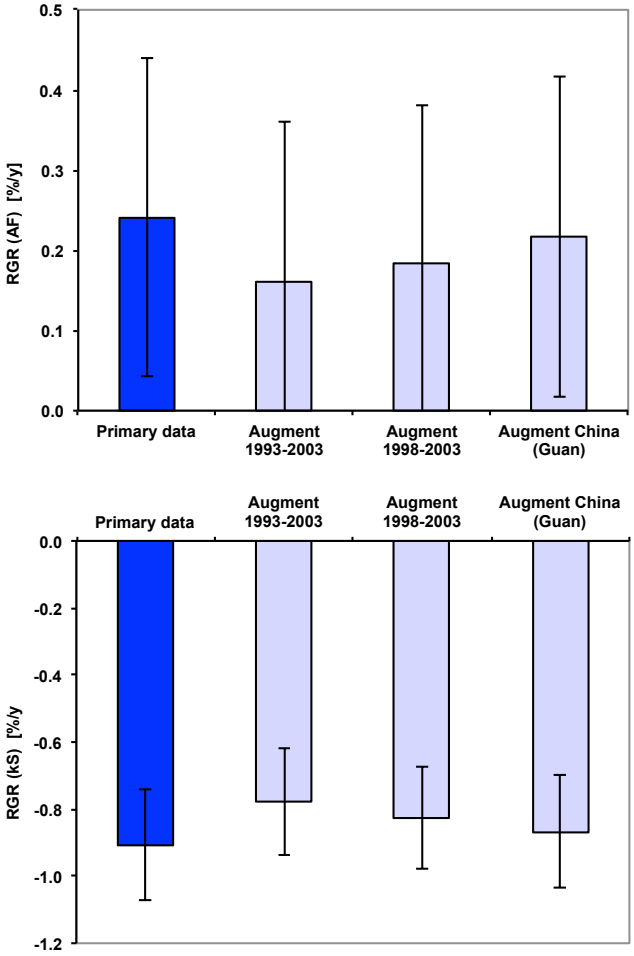

Figure D2. Estimates of RGR (AF) (upper panel) and RGR (k_S) (lower panel), using primary data for f_{Foss} (blue bars, as in Fig. 2) and three alternative f_{Foss} trajectories shown in Fig. D1 (pale grey bars). Trends are estimated using Eq. (A2). All estimates are computed using data treatment (m, s, n) and the combined trend detection method, as for best estimates (Fig. 2 and Tables 1 and 2). Error bars show $\pm 1\sigma$ confidence intervals. For RGR (AF), all P values (probability of positive trend) exceed 0.69; for RGR (k_S), all P values (probability of negative trend) exceed 0.996.

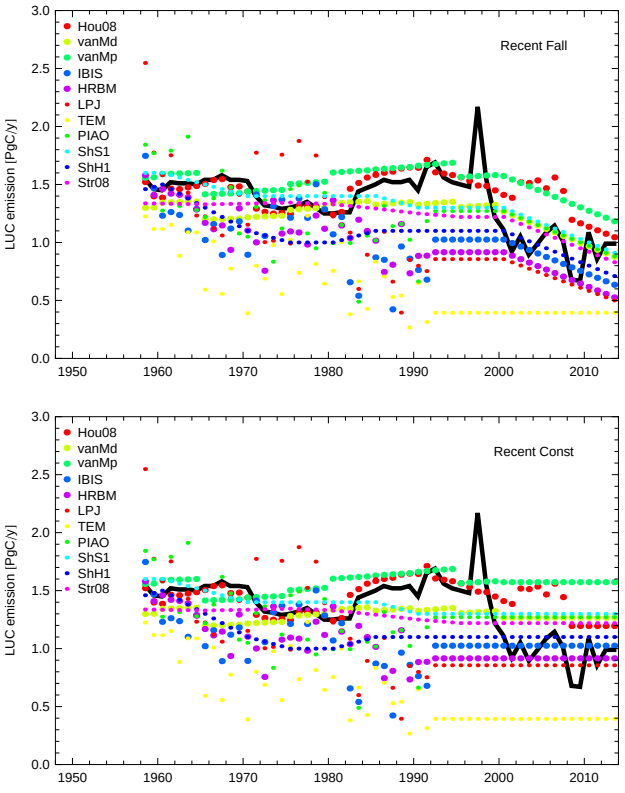

Figure D3. Alternative trajectories for CO_2 emissions from net land use change (f_{LUC}): (black) primary data; (coloured dots) alternative trajectories described in Table D1. Upper and lower panels show "Recent Fall" and "Recent Const" extrapolations, respectively.

uncertainty in AF trend estimates (Le Quéré et al., 2009; Raupach et al., 2008). The error on all f_{LUC} estimates is large, typically $\pm 50\,\%$. For estimation of both RGR (AF) and RGR (k_S), uncertainties arising from systematic biases in f_{LUC} data (both in level and trend) are more important than uncorrelated random errors in annual estimates. The primary data used here (Fig. C1) imply a downward revision of recent (since 2000) f_{LUC} from earlier estimates (Le Quéré et al., 2009). This is mainly attributable to methodological improvements in recently reported deforestation rates in the 2010 Food and Agriculture Organization (FAO) Forest Resources Assessment (FAO, 2010), relative to the 2005 assessment (FAO, 2006) used earlier (Le Quéré et al., 2009). In Brazil, estimates for deforestation rates are now based on high-resolution remote sensing imagery, while latest estimates for Indonesia are based on data for 2003 and 2006, in contrast with 2005 estimates based on forecasts for this period. Recent studies in parts of the world that have dominated global deforestation inventories in past decades, including Brazil (Nepstad et al., 2009; Regalado, 2011) and Indonesia (Hansen et al., 2008), support the hypothesis that f_{LUC} has declined significantly through 2000–2009.

To assess the implications of uncertainty in f_{LUC} for trends AF and k_S, we replaced the primary f_{LUC} data with 11 alternative annual time series from other assessments (Fig. D3 and Table D1). These alternative series are not independent, being based on just three sources of land cover data (FAO (FAO, 2010), SAGE (Ramankutty and Foley, 1999) and HYDE (Goldewijk, 2001)) and several carbon cycle models. Nevertheless, these series represent presently available estimates of global f_{LUC} from numerous investigators. All alternative f_{LUC} series end between 1990 and 2000, so each series was extrapolated in time by assuming either a linear decrease in f_{LUC} from 2000 onward at $0.03\,\mathrm{Pg\,C\,year^{-1}}$ per year consistent with our primary f_{LUC} data or a constant f_{LUC} from the end of each alternative f_{LUC} series (respectively denoted "Recent Fall" and "Recent Const" in Fig. D3).

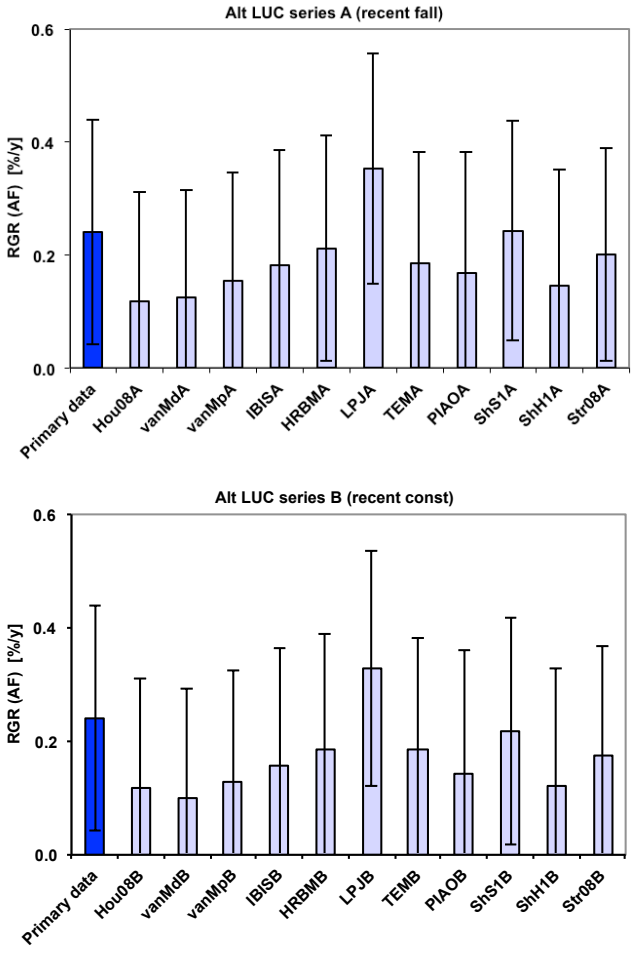

Figure D4. Estimates of RGR(AF) using primary data for f_{LUC} (blue bars) and 11 alternative f_{LUC} trajectories (Table D1 and Fig. D3, pale grey bars). Trends are estimated using Eq. (A2). P values are shown in Table D1. All estimates are computed using data treatment (m, s, n) and the combined trend detection method, as for best estimates in Fig. 2 and Tables 1 and 2. Error bars show $\pm 1\sigma$ confidence intervals. Upper and lower panels show RGR(AF) using "recent fall" and "recent const" extrapolations, respectively.

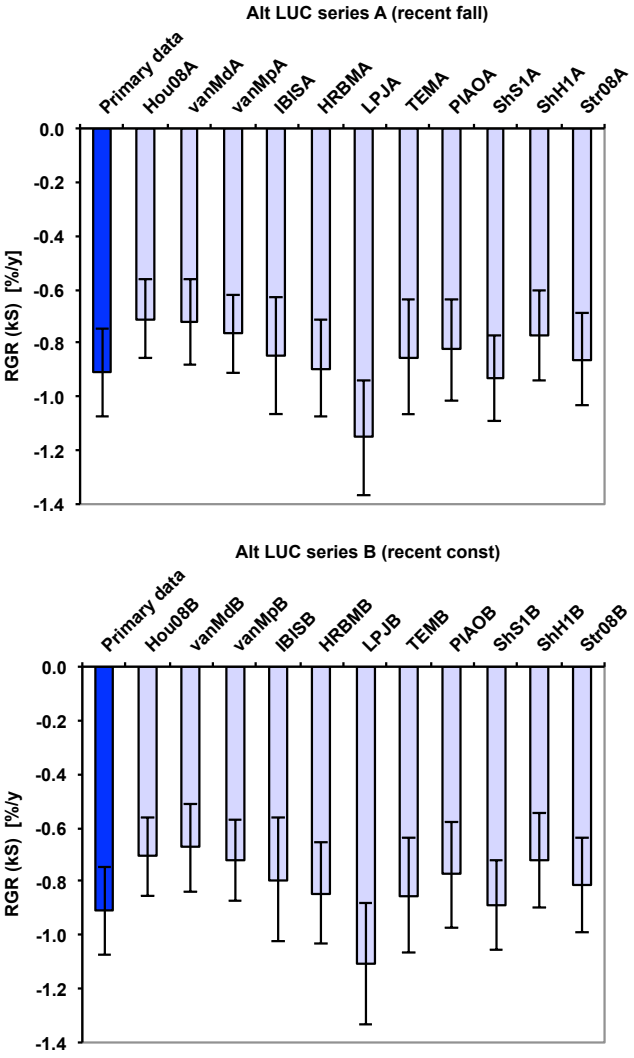

Figure D5. Estimates of RGR(k_{S}) using primary data for f_{LUC} (blue bars) and 11 alternative f_{LUC} trajectories (Table D1 and Fig. D3, pale grey bars). Trends are estimated using Eq. (A2). All P values (probability of negative k_{S} trend) exceed 0.98 (values not tabulated). Other details follow Fig. D4.

Because of the likely decline in f_{LUC} since 2000, "Recent Fall" is the more likely scenario.

The resulting trends RGR(AF) (Fig. D4) and RGR(k_{S}) (Fig. D5), computed using data treatment (m, s, n) and the combined trend detection method, are slightly smaller in magnitude than the best estimates with primary f_{LUC} data, but the differences are not statistically significant. This indicates that uncertainty in f_{LUC} does not significantly affect our results.

Acknowledgements. CO_2 data are provided by the Earth System Research Laboratory, US National Oceanic and Atmospheric Administration, and the CO_2 Program at the Scripps Institution of Oceanography. Data on fossil-fuel CO_2 emissions are provided by the Carbon Dioxide Information and Analysis Center (CDIAC), US Department of Energy. We thank W. Knorr for valuable comments. We acknowledge with gratitude the work of the C4MIP modelling community. We acknowledge support to M. R. Raupach and J. G. Canadell from the Australian Climate Change Science Programme of the Australian Government, to M. Gloor from the NERC consortium grant AMAZONICA (NE/F005806/1) and the European Union Seventh Framework Programme project GEOCARBON (grant number 283080), to J. L. Sarmiento from the Carbon Mitigation Initiative of Princeton University, to T. L. Frölicher from the SNSF (Ambizione grant PZ00P2_142573), and to C. Le Quéré from the European Union Seventh Framework Programme project CarboChange (grant number 264879). This work is a contribution to the Global Carbon Project.

Edited by: J. Middelburg

References

Ammann, C. M., Meehl, G. A., Washington, W. M., and Zender, C. S.: A monthly and latitudinally varying volcanic forcing dataset in simulations of 20th century climate, Geophys. Res. Lett., 30, 1657, doi:10.1029/2003GL016875, 2003.

Andres, R. J., Boden, T. A., Bréon, F.-M., Ciais, P., Davis, S., Erickson, D., Gregg, J. S., Jacobson, A., Marland, G., Miller, J., Oda, T., Olivier, J. G. J., Raupach, M. R., Rayner, P., and Treanton, K.: A synthesis of carbon dioxide emissions from fossil-fuel combustion, Biogeosciences, 9, 1845–1871, doi:10.5194/bg-9-1845-2012, 2012.

Archer, D., Eby, M., Brovkin, V., Ridgwell, A., Cao, L., Mikolajewicz, U., Caldeira, K., Matsumoto, K., Munhoven, G., Montenegro, A., and Tokos, K.: Atmospheric lifetime of fossil fuel carbon dioxide, Annu. Rev. Earth Pl. Sc., 37, 117–134, 2009.

Bacastow, R. B. and Keeling, C. D.: Models to predict future atmospheric CO_2 concentrations, in: Workshop on the Global Effects of Carbon Dioxide from Fossil Fuels, edited by: Elliott, W. P. and Machta, L., United States Department of Energy, Washington DC, 1979.

Ballantyne, A. P., Alden, C. B., Miller, J. B., Tans, P. P., and White, J. W. C.: Increase in observed net carbon dioxide uptake by land and oceans during the past 50 years, Nature, 488, 70–73, 2012.

Boden, T. A., Marland, G., and Andres, R. J.: Global, regional and national fossil-fuel CO_2 emissions, Carbon Dioxide Information Analysis Center, Oak Ridge National Laboratory, US Department of Energy, Oak Ridge, TN, USA, doi:10.3334/CDIAC/00001_V2013, http://cdiac.ornl.gov/trends/emis/meth_reg.html (last access: 23 November 2013), 2013.

Box, G., Jenkins, G. M., and Reinsel, G.: Time Series Analysis: Forecasting and Control, 3rd edn., Prentice Hall, Englewood Cliffs, NJ, 1994.

Canadell, J. G., Le Quéré, C., Raupach, M. R., Field, C. B., Buitenhuis, E. T., Ciais, P., Conway, T. J., Gillett, N. P., Houghton, R. A., and Marland, G.: Contributions to accelerating atmospheric CO_2 growth from economic activity, carbon intensity, and efficiency of natural sinks, P. Natl. Acad. Sci. USA, 104, 18866–18870, 2007.

Ciais, P., Gasser, T., Paris, J. D., Caldeira, K., Raupach, M. R., Canadell, J. G., Patwardhan, A., Friedlingstein, P., Piao, S., and Gitz, V.: Attributing the increase of atmospheric CO_2 to emitters and absorbers, Nat. Clim. Change, 3, 926–930, 2013.

FAO: Global Forest Resources Assessment 2005, Food and Agriculture Organization of the United Nations, Rome, 2006.

FAO: Global Forest Resources Assessment 2010, Food and Agriculture Organization of the United Nations, Rome, 2010.

Francey, R. J., Trudinger, C. M., van der Schoot, M., Krummel, P. B., Steele, L. P., and Langenfelds, R. L.: Differences between trends in atmospheric CO_2 and the reported trends in anthropogenic CO_2 emissions, Tellus B, 62, 316–328, 2010.

Friedlingstein, P., Cox, P., Betts, R., Bopp, L., von Bloh, W., Brovkin, V., Cadule, P., Doney, S., Eby, M., Fung, I., Bala, G., John, J., Jones, C., Joos, F., Kato, T., Kawamiya, M., Knorr, W., Lindsay, K., Matthews, H. D., Raddatz, T., Rayner, P., Reick, C., Roeckner, E., Schnitzler, K. G., Schnur, R., Strassmann, K., Weaver, A. J., Yoshikawa, C., and Zeng, N.: Climate–carbon cycle feedback analysis: results from the C4MIP model intercomparison, J. Climate, 19, 3337–3353, 2006.

Friedlingstein, P., Solomon, S., Plattner, G. K., Knutti, R., Ciais, P., and Raupach, M. R.: Long-term climate implications of twenty-first century options for carbon dioxide emission mitigation, Nat. Clim. Change, 1, 457-461, doi:10.1038/Nclimate1302, 2011.

Frölicher, T. L., Joos, F., Raible, C. C., and Sarmiento, J. L.: Atmospheric CO_2 response to volcanic eruptions: the role of ENSO, season, and variability, Global Biogeochem. Cy., 27, 239–251, 2013.

Gasser, T. and Ciais, P.: A theoretical framework for the net land-to-atmosphere CO_2 flux and its implications in the definition of "emissions from land-use change", Earth Syst. Dynam., 4, 171–186, doi:10.5194/esd-4-171-2013, 2013.

Gloor, M., Sarmiento, J. L., and Gruber, N.: What can be learned about carbon cycle climate feedbacks from the CO_2 airborne fraction?, Atmos. Chem. Phys., 10, 7739–7751, doi:10.5194/acp-10-7739-2010, 2010.

Goldewijk, K. K.: Estimating global land use change over the past 300 years: the HYDE database 1, Global Biogeochem. Cy., 15, 417–433, 2001.

Gregg, J. S., Andres, R. J., and Marland, G.: China: emissions pattern of the world leader in CO_2 emissions from fossil fuel consumption and cement production, Geophys. Res. Lett., 35, L08806, doi:10.1029/2007GL032887, 2008.

Guan, D., Lui, Z., Geng, Y., Lindner, S., and Hubacek, K.: The gigatonne gap in China's carbon dioxide inventories, Nat. Clim. Change, 2, 672–675, doi:10.1038/NCLIMATE1560, 2012.

Hansen, M. C., Stehman, S. V., Potapov, P. V., Loveland, T. R., Townshend, J. R. G., DeFries, R. S., Pittman, K. W., Arunarwati, B., Stolle, F., Steininger, M. K., Carroll, M., and DiMiceli, C.: Humid tropical forest clearing from 2000 to 2005 quantified by using multitemporal and multiresolution remotely sensed data, P. Natl. Acad. Sci. USA, 105, 9439–9444, 2008.

Harman, I. N., Trudinger, C. M., and Raupach, M. R.: SCCM – the Simple Carbon–Climate Model: Technical documentation, Centre for Australian Weather and Climate Research, Bureau of Meteorology and CSIRO, Melbourne, Australia, 2011.

Hofmann, D. J., Butler, J. H., and Tans, P. P.: A new look at atmospheric carbon dioxide, Atmos. Environ., 43, 2084–2086, 2009.

Houghton, R. A.: Why are estimates of the terrestrial carbon balance so different?, Glob. Change Biol., 9, 500–509, 2003.

Houghton, R. A.: How well do we know the flux of CO_2 from land-use change?, Tellus B, 62, 337–351, 2010.

IPCC: Climate Change 2007: Synthesis Report, Cambridge University Press, Cambridge, UK and New York, NY, USA, 2007.

Jones, C. D. and Cox, P. M.: Modeling the volcanic signal in the atmospheric CO_2 record, Global Biogeochem. Cy., 15, 453–465, 2001.

Joos, F., Bruno, M., Fink, R., Siegenthaler, U., Stocker, T. F., and Le Quéré, C.: An efficient and accurate representation of complex oceanic and biospheric models of anthropogenic carbon uptake, Tellus B, 48, 397–417, 1996.

Joos, F., Roth, R., Fuglestvedt, J. S., Peters, G. P., Enting, I. G., von Bloh, W., Brovkin, V., Burke, E. J., Eby, M., Edwards, N. R., Friedrich, T., Frölicher, T. L., Halloran, P. R., Holden, P. B., Jones, C., Kleinen, T., Mackenzie, F. T., Matsumoto, K., Meinshausen, M., Plattner, G.-K., Reisinger, A., Segschneider, J., Shaffer, G., Steinacher, M., Strassmann, K., Tanaka, K., Timmermann, A., and Weaver, A. J.: Carbon dioxide and climate impulse response functions for the computation of greenhouse gas metrics: a multi-model analysis, Atmos. Chem. Phys., 13, 2793–2825, doi:10.5194/acp-13-2793-2013, 2013.

Keeling, C. D. and Revelle, R.: Effects of El-Nino Southern Oscillation on the atmospheric content of carbon-dioxide, Meteoritics, 20, 437–450, 1985.

Keeling, C. D., Piper, S. C., Bacastow, R. B., Wahlen, M., Whorf, T. P., Heimann, M., and Meijer, H. A.: Exchanges of Atmospheric CO_2 and $^{13}CO_2$ with the Terrestrial Biosphere and Oceans From 1978 to 2000. I. Global Aspects, Scripps Institution of Oceanography, San Diego, 88 pp., 2001.

Keeling, C. D., Piper, S. C., Bacastow, R. B., Wahlen, M., Whorf, T. P., Heimann, M., and Meijer, H. A.: Atmospheric CO_2 and $^{13}CO_2$ exchange with the terrestrial biosphere and oceans from 1978 to 2000: observations and carbon cycle implications, in: A History of Atmospheric CO_2 and Its Effects on Plants, Animals, and Ecosystems, edited by: Ehleringer, J. R., Cerling, T. E., and Dearing, M. D., Springer Verlag, New York, 2005.

Knorr, W.: Is the airborne fraction of anthropogenic CO_2 emissions increasing?, Geophys. Res. Lett., 36, L21710, doi:10.1029/2009GL040613, 2009.

Le Quéré, C., Rodenbeck, C., Buitenhuis, E. T., Conway, T. J., Langenfelds, R., Gomez, A., Labuschagne, C., Ramonet, M., Nakazawa, T., Metzl, N., Gillett, N., and Heimann, M.: Saturation of the Southern Ocean CO_2 sink due to recent climate change, Science, 316, 1735–1738, 2007.

Le Quéré, C., Raupach, M. R., Canadell, J. G., Marland, G., Bopp, L., Ciais, P., Conway, T. J., Doney, S. C., Feely, R. A., Foster, P., Friedlingstein, P., Gurney, K. R., Houghton, R. A., House, J. I., Huntingford, C., Levy, P. E., Lomas, M. R., Majkut, J., Metzl, N., Ometto, J., Peters, G. P., Prentice, I. C., Randerson, J. T., Running, S. W., Sarmiento, J. L., Schuster, U., Sitch, S., Takahashi, T., Viovy, N., van der Werf, G. R., and Woodward, F. I.: Trends in the sources and sinks of carbon dioxide, Nat. Geosci., 2, 831–836, 2009.

Le Quéré, C., Andres, R. J., Boden, T., Conway, T., Houghton, R. A., House, J. I., Marland, G., Peters, G. P., van der Werf, G. R., Ahlström, A., Andrew, R. M., Bopp, L., Canadell, J. G., Ciais, P., Doney, S. C., Enright, C., Friedlingstein, P., Huntingford, C., Jain, A. K., Jourdain, C., Kato, E., Keeling, R. F., Klein Goldewijk, K., Levis, S., Levy, P., Lomas, M., Poulter, B., Raupach, M. R., Schwinger, J., Sitch, S., Stocker, B. D., Viovy, N., Zaehle, S., and Zeng, N.: The global carbon budget 1959–2011, Earth Syst. Sci. Data, 5, 165–185, doi:10.5194/essd-5-165-2013, 2013.

Lewis, E. and Wallace, D. J.: Program Developed for CO_2 System Calculations, Carbon Dioxide Information Analysis Center, Oak Ridge National Laboratory, Oak Ridge, Tennessee, 38 pp., 1998.

Li, S. and Jarvis, A. J.: Long run surface temperature dynamics of an A-OGCM: the HadCM3 4xCO_2 forcing experiment revisited, Clim. Dynam., 33, 817–825, 2009.

Li, S., Jarvis, A. J., and Leedal, D. T.: Are response function representations of the global carbon cycle ever interpretable?, Tellus B-Chem. Phys. Meteorol., 61, 361–371, 2009.

Marland, G.: Uncertainties in accounting for CO_2 from fossil fuels, J. Ind. Ecol., 12, 136–139, 2008.

McGuire, A. D., Sitch, S., Clein, J. S., Dargaville, R., Esser, G., Foley, J. A., Heimann, M., Joos, F., Kaplan, J., Kicklighter, D. W., Meier, R. A., Melillo, J. M., Moore, B., Prentice, I. C., Ramankutty, N., Reichenau, T., Schloss, A., Tian, H., Williams, L. J., and Wittenberg, U.: Carbon balance of the terrestrial biosphere in the twentieth century: analyses of CO_2, climate and land use effects with four process-based ecosystem models 1, Global Biogeochem. Cy., 15, 183–206, 2001.

Millennium Ecosystem Assessment: Ecosystems and human well-being: synthesis, Island Press, Washington DC, USA, 2005.

Nepstad, D., Soares, B. S., Merry, F., Lima, A., Moutinho, P., Carter, J., Bowman, M., Cattaneo, A., Rodrigues, H., Schwartzman, S., McGrath, D. G., Stickler, C. M., Lubowski, R., Piris-Cabezas, P., Rivero, S., Alencar, A., Almeida, O., and Stella, O.: The end of deforestation in the Brazilian Amazon, Science, 326, 1350–1351, 2009.

NOAA-ESRL: Trends in Atmospheric Carbon Dioxide, Global Monitoring Division, Earth System Research Laboratory, National Oceanic and Atmospheric Admisinstration, Boulder, CO, USA, http://www.esrl.noaa.gov/gmd/ccgg/trends/ (last access: 23 November 2013), 2013.

Oeschger, H., Siegenthaler, U., and Heimann, M.: The carbon cycle and its perturbations by man, in: Interactions of Energy and Climate, edited by: Bach, W., Pankrath, J., and Williams, J., Reidel, Dordrecht, 1980.

Piao, S. L., Ciais, P., Friedlingstein, P., de Noblet-Ducoudre, N., Cadule, P., Viovy, N., and Wang, T.: Spatiotemporal patterns of terrestrial carbon cycle during the 20th century, Global Biogeochem. Cy., 23, GB4026, doi:10.1029/2008GB003339, 2009.

Ramankutty, N. and Foley, J. A.: Estimating historical changes in global land cover: croplands from 1700 to 1992, Global Biogeochem. Cy., 13, 997–1027, 1999.

Raupach, M. R.: The exponential eigenmodes of the carbon–climate system, and their implications for ratios of responses to forcings, Earth Syst. Dynam., 4, 31–49, doi:10.5194/esd-4-31-2013, 2013.

Raupach, M. R., Canadell, J. G., and Le Quéré, C.: Anthropogenic and biophysical contributions to increasing atmospheric CO_2 growth rate and airborne fraction, Biogeosciences, 5, 1601–1613, doi:10.5194/bg-5-1601-2008, 2008.

Raupach, M. R., Canadell, J. G., Ciais, P., Friedlingstein, P., Rayner, P. J., and Trudinger, C. M.: The relationship between peak warming and cumulative CO_2 emissions, and its use to quantify vulnerabilities in the carbon–climate–human system, Tellus B, 63, 145–164, 2011.

Regalado, A.: Brazil says rate of deforestation in the Amazon continues to plunge, Science, 329, 1270–1271, 2011.

Sarmiento, J. L., Gloor, M., Gruber, N., Beaulieu, C., Jacobson, A. R., Mikaloff Fletcher, S. E., Pacala, S., and Rodgers, K.: Trends and regional distributions of land and ocean carbon sinks, Biogeosciences, 7, 2351–2367, doi:10.5194/bg-7-2351-2010, 2010.

Scripps CO_2 Program: Atmospheric CO_2 data, Scripps Institution of Oceanography, San Diego, CA, USA, http://scrippsco2.ucsd.edu/data/data.html, (last access: 23 November 2013), 2013.

Shevliakova, E., Pacala, S. W., Malyshev, S., Hurtt, G. C., Milly, P. C. D., Caspersen, J. P., Sentman, L. T., Fisk, J. P., Wirth, C., and Crevoisier, C.: Carbon cycling under 300 years of land use change: importance of the secondary vegetation sink 1, Global Biogeochem. Cy., 23, GB2022, doi:10.1029/2007GB003176, 2009.

Sitch, S., Friedlingstein, P., Gruber, N., Jones, S. D., Murray-Tortarolo, G., Ahlström, A., Doney, S., Graven, H., Heinze, C., Huntingford, C., Levis, S., Levy, P., Lomas, M., Poulter, B., Viovy, N., Zaehle, S., Zeng, N., Arneth, A., Bonan, G., Bopp, L., Canadell, J. G., Chevallier, F., Ciais, P., Ellis, R., Gloor, M., Peylin, P., Piao, S., Le Quéré, C., Smith, B., Zhu, Z., and Myneni, R.: Trends and drivers of regional sources and sinks of carbon dioxide over the past two decades, Biogeosciences Discuss., 10, 20113–20177, doi:10.5194/bgd-10-20113-2013, 2013.

Strassmann, K. M., Joos, F., and Fischer, G.: Simulating effects of land use changes on carbon fluxes: past contributions to atmospheric CO_2 increases and future commitments due to losses of terrestrial sink capacity 1, Tellus B, 60, 583–603, 2008.

Tans, P.: An accounting of the observed increase in oceanic and atmospheric CO_2 and an outlook for the future, Oceanography, 22, 26–35, 2009.

UNFCCC: Methodological Issues: Scientific and Methodological Assessment of Contributions to Climate Change, Subsidiary Body for Scientific and Technological Advice, United Nations Framework Convention on Climate Change, New Delhi, 27 pp., 2002.

Van Minnen, J. G., Goldewijk, K. K., Stehfest, E., Eickhout, B., Van Drecht, G., and Leemans, R.: The importance of three centuries of land-use change for the global and regional terrestrial carbon cycle, Climatic Change, 97, 123–144, 2009.